HIERARCHICAL MODEL REDUCTION DRIVEN BY A PROPER ORTHOGONAL DECOMPOSITION FOR PARAMETRIZED ADVECTION-DIFFUSION-REACTION PROBLEMS*

MASSIMILIANO LUPO PASINI† AND SIMONA PEROTTO‡

Abstract. This work combines the Hierarchical Model (HiMod) reduction technique with a standard Proper Orthogonal Decomposition (POD) to solve parametrized partial differential equations for the modeling of advection-diffusion-reaction phenomena in elongated domains (e.g., pipes). This combination leads to what we define a HiPOD model reduction, which merges the reliability of HiMod reduction with the computational efficiency of POD. Two HiPOD techniques are presented and assessed through an extensive numerical verification.

Key words. hierarchical model reduction, proper orthogonal decomposition, parametric partial differential equations, finite elements, spectral methods

AMS subject classifications. 65N30, 65N35, 65T40

1. Motivations. Parametrized partial differential equations (PDEs) arise in several contexts such as inverse problems, control, optimization, uncertainty quantification, and risk assessment. In most of these applications, the number of parameters may become very large, so that an efficient numerical approximation of parametric PDEs represents a challenging computational issue (see, e.g., [2, 6, 7, 3]). Parametric model order reduction aims at reducing the computational effort associated with a parametric modeling, for instance, in many-query and real-time tasks, where the occurrence of the curse of dimensionality raises the necessity to propose numerical methods to sustain the computational cost.

Many of the model reduction techniques currently employed in engineering practice exploit the offline/online paradigm to efficiently reduce the numerical effort. This is the case, for instance, of the well-known reduced basis method [17, 33], where, during the offline phase, a reduced basis is precomputed by solving a high-fidelity model (the "truth") for certain samples of the parameter, while, in the online phase, the reduced model is evaluated to predict a new scenario (i.e., for a value of the parameter not previously sampled). From a practical viewpoint, the offline stage remains the bottleneck of an offline/online decomposition, especially when many samples are needed like for multiparametric problems.

To tackle this issue, we propose to replace the "truth" with a reduced order model which exhibits a high accuracy although characterized by a contained computational demand. For this purpose, we employ the reduced solution provided by a Hierarchical Model (HiMod) discretization [12, 28, 31, 26] as high fidelity model.
HiMod reduction proved to be an effective tool to model partial differential problems characterized by a privileged dynamics aligned with the dominant dimension of the domain (e.g., flows of fluid in channels, pipes or vessels), which may be locally modified by secondary dynamics

*

†Computational Sciences and Engineering Division, Oak Ridge National Laboratory, 1 Bethel Valley Road, Oak Ridge, TN, USA, 37831 (`lupopasinim@ornl.gov`).

‡MOX – Dipartimento di Matematica, Politecnico di Milano, Piazza L. da Vinci 32, I-20133 Milano, Italy (`simona.perotto@polimi.it`).

ETNA
Kent State University and
Johann Radon Institute (RICAM)

evolving along the transverse sections [29, 15, 8]. Analogously to other model reduction procedures [34, 9, 16, 14, 10, 24], a HiMod discretization moves from a standard separation of variables and approximates the mainstream and the secondary dynamics by means of different numerical methods. In the seminal papers, the main direction of the flux is discretized by one-dimensional (1D) finite elements, while the transverse dynamics are recovered by using few degrees of freedom, via a suitable modal basis. This separate discretization yields a system of coupled 1D problems, whose coefficients include the effect of the transverse dynamics. The reliability exhibited by HiMod is considerably higher compared with standard 1D reduced models, whereas the computational effort remains absolutely affordable. Indeed, HiMod reduction is characterized by a linear dependence of the computational cost on the number of degrees of freedom, in contrast to a standard finite element model which demands a suitable power of such a number.

In this paper, we focus on two different ways to combine Proper Orthogonal Decomposition (POD) [21, 22, 20, 19, 36] with HiMod reduction, setting what we define as HiPOD model reduction. The first approach is very straightforward and it has been introduced in [4]. The second variant, which represents the actual novelty of the paper, is more complex and takes advantage of the separation of variables implied by a HiMod approximation. Independently of the adopted procedure, the HiMod discretization significantly reduces the computational effort of the offline phase without compromising its reliability. At the same time, the online phase relies on the efficiency of a POD formulation, so that a system of very small dimensionality is solved to approximate the parametric problem at hand.

From a different viewpoint, we can conceive HiPOD as a new method to construct HiMod approximations, which differs from the classical approach proposed in [12, 28]. The HiMod approximation is now built by resorting to a reduced basis generated by a data-driven procedure. This choice significantly lowers the computational costs without compromising the quality of the reduced solution.

The paper is organized as follows. Section 2 applies the HiMod discretization to a reference parametric advection-diffusion-reaction problem and numerically assesses the reliability of the high-fidelity model. Section 3 introduces the two HiPOD model reduction procedures, and provides an extensive numerical verification to investigate the robustness of the proposed approaches with respect to the truncation of the POD basis, the extrapolation, and the possibility to explore multi-parametric settings. In Section 4 we look for possible settings where one of the two HiPOD approximations outperforms the other. Finally, some conclusions are drawn in the last section, and possible future developments of the current work are provided.

2. HiMod reduction: the basic. HiMod reduction is performed under the specific assumption that the computational domain, $\Omega \subset \mathbb{R}^d$ with $d = 2, 3$, can be expressed as a Cartesian product, $\bigcup_{x\in\Omega_{1D}} \{x\} \times \Sigma_x$, where Ω_{1D} is a 1D horizontal supporting fiber, while $\Sigma_x \subset \mathbb{R}^{d-1}$ denotes the transverse section at the generic point x along Ω_{1D} [12, 28, 31, 26]. The reference geometry is a pipe, where the dominant dynamic is parallel to Ω_{1D}, whereas the transverse dynamics occur along fibers Σ_x. For the sake of simplicity, we select $\Omega_{1D} \equiv (a, b) \subset \mathbb{R}$. For the general case where Ω_{1D} coincides with a bent centerline, we refer to [25, 29, 8]. Then, via an invertible map $\Psi : \Omega \to \widehat{\Omega}$, we change the physical domain Ω into a reference domain $\widehat{\Omega} = \Omega_{1D} \times \widehat{\Sigma}$, which shares the same supporting fiber as in Ω, and where $\widehat{\Sigma} \subset \mathbb{R}^{d-1}$ denotes the reference fiber. In particular, for any point $\mathbf{z} = (x, \mathbf{y}) \in \Omega$, there exists a point $\widehat{\mathbf{z}} = (\widehat{x}, \widehat{\mathbf{y}}) \in \widehat{\Omega}$, such that $\widehat{\mathbf{z}} = \Psi(\mathbf{z})$, with $\widehat{x} \equiv x$ and $\widehat{\mathbf{y}} = \psi_x(\mathbf{y})$, where $\psi_x : \Sigma_x \to \widehat{\Sigma}$ is the map between the generic and the reference transverse fiber. Hereafter, we assume ψ_x to be a C^1-diffeomorphism for all $x \in \Omega_{1D}$, and Ψ to be differentiable with respect to $\mathbf{z}$. The reference domain $\widehat{\Omega}$ represents the setting where the computations are actually performed, and

ETNA
Kent State University and
Johann Radon Institute (RICAM)

where all the constants can be explicitly computed. More details about maps Ψ and ψ_x are available in [28].

As a reference problem, we choose a parametrized elliptic PDE, defined on Ω, which can be recast into the following weak form: given the parameter $\alpha \in \mathcal{P}$,

$$\text{find } u(\alpha) \in V \quad \text{s.t.} \quad a(u(\alpha), v; \alpha) = f(v; \alpha) \quad \forall v \in V, \tag{2.1}$$

where $\mathcal{P} \subset \mathbb{R}^p$ is the set of the admissible parameters; $V \subseteq H^1(\Omega)$ is a Hilbert space depending on the PDE problem and on the selected boundary conditions, with standard notation for function spaces [11]; $a(\cdot, \cdot; \alpha) : V \times V \times \mathcal{P} \to \mathbb{R}$ and $f(\cdot; \alpha) : V \times \mathcal{P} \to \mathbb{R}$ denote a parametrized bilinear and linear form, respectively, where the linearity property holds with respect to all the variables but α. Suitable hypotheses are imposed on the problem data to guarantee the well-posedness of formulation (2.1), for any $\alpha \in \mathcal{P}$. Moreover, we assume an affine parameter dependence [17, 33].

We focus on a scalar linear advection-diffusion-reaction (ADR) problem completed, for the sake of simplicity, with full homogeneous Dirichlet boundary conditions, so that the bilinear and the linear forms in (2.1) are

$$a(w, z; \alpha) = \int_\Omega \mu \nabla w \cdot \nabla z \, d\Omega + \int_\Omega \big(\mathbf{b} \cdot \nabla w + \sigma w\big) z \, d\Omega, \quad f(z; \alpha) = \int_\Omega f z \, d\Omega, \tag{2.2}$$

with $w, z \in V = H^1_0(\Omega)$. The parameter α coincides with one or several of the problem data, chosen among the viscosity μ, the advective field $\mathbf{b} = [b_1, \dots, b_d]^T$, the reaction coefficient σ, the source term f, or a boundary value when boundary conditions, more general with respect to the homogeneous Dirichlet data, are assigned.

HiMod reduction performs a different discretization along the supporting and the transverse directions. For this purpose, we introduce a 1D discrete space, $V_{1D} \subset H^1_0(\Omega_{1D})$ with $\dim(V_{1D}) = N_h < +\infty$, of functions vanishing at a and b, and a modal basis $\{\varphi_k\}_{k \in \mathbb{N}^+}$ of functions defined on $\widehat{\Sigma}$ which are orthonormal with respect to the $L^2(\widehat{\Sigma})$-scalar product and which satisfy the data assigned on $\Gamma_L = \cup_{x \in \Omega_{1D}} \partial\Sigma_x$. For further details about the choice of the modal basis, also in the presence of general boundary data on Γ_L, we refer to [1, 15, 28]. Concerning V_{1D}, a standard choice is the finite element space [12, 28, 31, 26, 30, 32] or an isogeometric discretization when Ω is not rectilinear [29, 8]. Thus, the HiMod reduced space can be defined as

$$V_m = \Big\{ v_m(x, \mathbf{y}; \alpha) = \sum_{k=1}^{m} \sum_{j=1}^{N_h} \widetilde{v}^{\alpha}_{k,j} \vartheta_j(x) \varphi_k(\psi_x(\mathbf{y})), \text{ for } x \in \Omega_{1D}, \mathbf{y} \in \Sigma_x, \alpha \in \mathcal{P} \Big\},$$

with $\{\vartheta_j\}_{j=1}^{N_h}$ a basis for the space V_{1D}, so that $\widetilde{v}_k(x; \alpha) = \sum_{j=1}^{N_h} \widetilde{v}^{\alpha}_{k,j} \vartheta_j(x) \in V_{1D}$ denotes the frequency coefficient of v_m associated with the k-th modal function φ_k.

The modal index $m \in \mathbb{N}^+$ establishes the level of detail of the HiMod approximation in the hierarchy, $\{V_m\}_m$, of reduced spaces. This index is selected by the user through some preliminary (geometric or physical) information about the problem at hand, or via an automatic procedure based on an a posteriori modeling error analysis [30, 32]. Additionally, index m can be the same in the whole Ω, or it can be locally tuned along the domain to match possible heterogeneities of the solution. We refer the interested reader to [31, 26], where a survey about the different criteria to choose m is provided.

The HiMod approximation to problem (2.1) becomes

$$\text{find } u_m(\alpha) = u_m(x, \mathbf{y}; \alpha) \in V_m \quad \text{s.t.} \quad a(u_m(\alpha), v_m; \alpha) = f(v_m; \alpha) \quad \forall v_m \in V_m, \tag{2.3}$$

ETNA
Kent State University and
Johann Radon Institute (RICAM)

for a given parameter $\alpha \in \mathcal{P}$ and for a selected modal index $m \in \mathbb{N}^+$. Following [28], we add a conformity and a spectral approximability assumption on the HiMod space, V_m, to ensure the well-posedness of formulation (2.3), along with a standard density assumption on space V_{1D} to guarantee the convergence of the HiMod approximation $u_m(\alpha)$ to the full solution $u(\alpha)$ in (2.1). From a computational viewpoint, after applying the HiMod expansion to the solution $u_m(\alpha)$ in (2.3) and choosing the test function v_m as the generic product $\vartheta_t \varphi_q$, with $q = 1, \dots, m$ and $t = 1, \dots, N_h$, the HiMod formulation turns into the system

$$A_m(\alpha)\mathbf{u}_m(\alpha) = \mathbf{f}_m(\alpha), \tag{2.4}$$

of m 1D coupled problems, where $A_m(\alpha) \in \mathbb{R}^{mN_h \times mN_h}$ and $\mathbf{f}_m(\alpha) \in \mathbb{R}^{mN_h}$ are the HiMod stiffness matrix and right-hand side, while

$$\mathbf{u}_m(\alpha) = \left[\widetilde{u}^{\alpha}_{1,1}, \dots, \widetilde{u}^{\alpha}_{1,N_h}, \widetilde{u}^{\alpha}_{2,1}, \dots, \widetilde{u}^{\alpha}_{2,N_h}, \dots, \widetilde{u}^{\alpha}_{m,1}, \dots, \widetilde{u}^{\alpha}_{m,N_h}\right]^T \in \mathbb{R}^{mN_h}$$

is the vector describing the solution,

$$u_m(x, \mathbf{y}; \alpha) = \sum_{k=1}^{m} \sum_{j=1}^{N_h} \widetilde{u}^{\alpha}_{k,j} \vartheta_j(x) \varphi_k(\psi_x(\mathbf{y})), \tag{2.5}$$

discretized via the HiMod approach, where $\{\widetilde{u}^{\alpha}_{k,j}\}_{k=1,j=1}^{m,N_h}$ are the modal coefficients (see [12, 28] for additional computational details).

When the mainstream dominates the transverse dynamics (i.e., for small values of m), the HiMod procedure has been shown to considerably reduce the computational burden associated with a standard discretization of problem (2.1), without affecting the accuracy of the simulation [23, 15, 8].

2.1. Reliability check of the HiMod reduction. The numerical assessment of this paper focuses on the two-dimensional (2D) setting. In this section, we qualitatively investigate the reliability of the HiMod reduction on two ADR problems completed with different boundary conditions, and we disregard the role played by the PDE parameters at this stage. For the HiMod discretization, we resort to linear finite elements (FE) along Ω_{1D}, whereas we describe the transverse dynamics with a sinusoidal modal basis. For a quantitative analysis as well as for a three-dimensional (3D) verification of the HiMod approximation, we refer the reader to [28, 1, 15, 8].

2.1.1. Test case 1. We define the domain Ω as the rectangle $(0, 3) \times (0, 1)$, while the problem data in (2.2) are

$$\mu(x, y) = 1, \quad \mathbf{b}(x, y) = [3, 0]^T, \quad \sigma(x, y) = 0, \quad f(x, y) = 1 - 2x + 3y. \tag{2.6}$$

The image at the top of Figure 2.1 shows the reference (full) solution computed with linear FE on a uniform unstructured grid of 260058 triangles. The chosen data justify the diffusive trend of the solution, which alternates a maximum to a minimum area.

With regards to the HiMod approximation, we subdivide the supporting fiber $[0, 3]$ into 60 uniform subintervals and we discretize the transverse dynamics by gradually increasing the number, m, of modal basis functions. The bottom panels in Figure 2.1 show the HiMod approximations for $m = 1$ (left) and $m = 2$ (right). It is evident that two modes are enough for ensuring a qualitatively good accuracy to the reduced solution, with a considerable reduction in terms of degrees of freedom (dofs) (120 dofs for the HiMod approximation to be compared with 373464 dofs for the FE model).

ETNA
Kent State University and
Johann Radon Institute (RICAM)

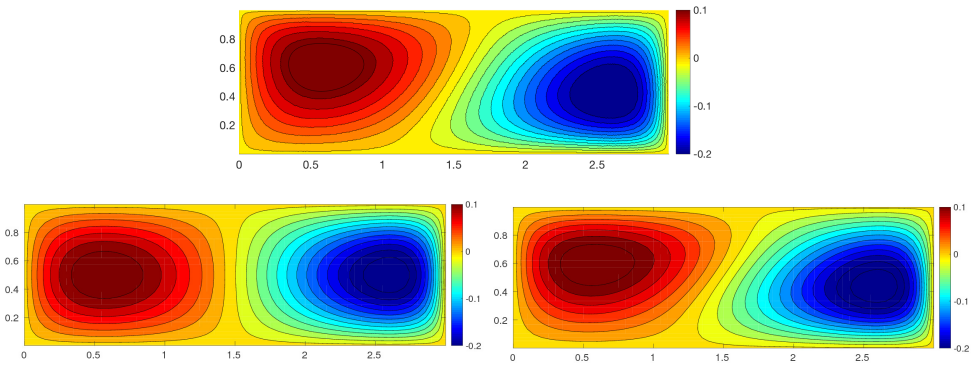

Fig. 2.1: HiMod verification (test case 1): reference FE (top) and HiMod (bottom) solution for $m = 1$ (left) and $m = 2$ (right).

2.1.2. Test case 2. The domain Ω is now taken as the rectangle $(0, 6) \times (0, 1)$ and we select the problem data as

$$\begin{aligned} \mu(x, y) = 0.24, \quad \mathbf{b}(x, y) = [5, \sin(6x)]^T, \quad \sigma(x, y) = 0.1, \\ f(x, y) = 10\chi_{C_1}(x, y) + 10\chi_{C_2}(x, y), \end{aligned} \tag{2.7}$$

where χ_ω denotes the characteristic function associated with the generic region $\omega \subset \mathbb{R}^2$, while C_1 and C_2 identify the ellipsoidal areas $\{(x, y) : (x - 0.75)^2 + 0.4(y - 0.25)^2 < 0.01\}$ and $\{(x, y) : (x - 0.75)^2 + 0.4(y - 0.75)^2 < 0.01\}$, respectively. The ADR problem is completed with a homogeneous Neumann data on $\Gamma_N = \{(x, y) : x = 6, 0 \le y \le 1\}$ and by a homogeneous Dirichlet condition on $\Gamma_D = \partial\Omega \setminus \Gamma_N$, so that $V \equiv H^1_{\Gamma_D}(\Omega)$ in (2.1). The top panel of Figure 2.2 displays the contour plot of the approximation obtained with linear FE on a uniform and unstructured mesh consisting of 3200 elements. We draw the attention of the reader to the oscillatory dynamics induced by the sinusoidal field, and the presence of the two localized sources in C_1 and C_2. Moreover, no stabilization is applied, despite the convection overcomes the diffusion. HiMod reduction is applied by introducing a uniform subdivision of Ω_{1D} into 120 subintervals and by employing an increasing number of modes. We do not introduce any stabilization also for the HiMod discretization. Figure 2.2, second-fourth row, shows the HiMod approximation for $m = 2$, $m = 3$ and $m = 5$, respectively. At least five modes have to be employed to obtain a qualitatively reliable HiMod solution. As expected, the number of HiMod dofs is considerably lower compared with the FE case (600 versus 305171 dofs).

3. HiPOD techniques. The goal of the HiPOD techniques is to build a HiMod approximation for problem (2.1) at a computational cost lower with respect to the one characterizing the HiMod system (2.4). For this purpose, we resort to a POD approach, by adopting the offline/online paradigm [21, 22, 20, 19, 36]. In particular, during the offline phase, we discretize problem (2.1) via HiMod for different choices of α, to extract the POD (reduced) basis; in the online phase, we employ such a basis to approximate the HiMod solution to (2.1) for a value, $\alpha = \alpha^*$, of the parameter not yet sampled.

In this paper we explore two different HiPOD approaches. The first one is the most straightforward procedure, where the online phase is carried out by resorting to a standard projection [4]. In the second approach, we drive the online phase by means of interpolation, following [37]. This second variant takes advantage of the separation of variables implied by

ETNA
Kent State University and
Johann Radon Institute (RICAM)

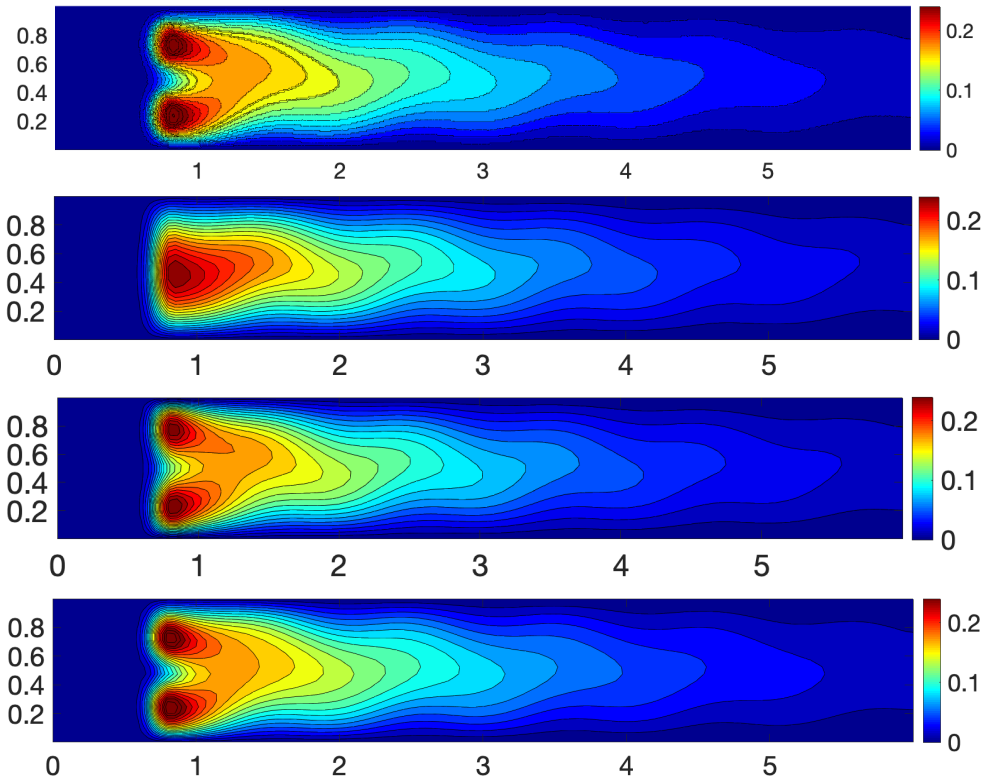

Fig. 2.2: HiMod verification (test case 2): reference FE (first row) and HiMod solution for $m = 2$ (second row), $m = 3$ (third row) and $m = 5$ (fourth row).

a HiMod discretization.
The leading feature of a HiPOD technique is to contain the computational burden typical of an offline phase. Actually, the POD is applied to solutions which have already been reduced via HiMod, in contrast to standard approaches where full solutions (e.g., finite element approximations) are employed to sample the phenomenon at hand. Finally, we notice that HiPOD methods are fully general since, a priori, any model reduction technique may replace the HiMod discretization during the offline phase.

3.1. The basic HiPOD approach. We start the *offline phase* by assembling the snapshot (or response) matrix S. To this aim, we select p different values, α_i, of the parameter α, and we compute the HiMod approximation to the associated problem (2.1), for $i = 1, \dots, p$. We employ the same discretization along Ω_{1D} and the same modal expansion for the transverse dynamics, so that, according to representation (2.5), each HiMod solution is identified by the mN_h coefficients $\{\widetilde{u}_{k,j}^{\alpha_i}\}_{k=1,j=1}^{m,N_h}$ or, likewise, by vector

$$\mathbf{u}_m(\alpha_i) = \big[\underbrace{\widetilde{u}_{1,1}^{\alpha_i}, \dots, \widetilde{u}_{1,N_h}^{\alpha_i}}_{k=1}, \underbrace{\widetilde{u}_{2,1}^{\alpha_i}, \dots, \widetilde{u}_{2,N_h}^{\alpha_i}}_{k=2}, \dots, \underbrace{\widetilde{u}_{m,1}^{\alpha_i}, \dots, \widetilde{u}_{m,N_h}^{\alpha_i}}_{k=m}\big]^T \in \mathbb{R}^{mN_h}, \tag{3.1}$$

collecting the modal coefficients by mode. Thus, we assemble the snapshot matrix

$$S = \big[\mathbf{u}_m(\alpha_1), \mathbf{u}_m(\alpha_2), \dots, \mathbf{u}_m(\alpha_p)\big] \in \mathbb{R}^{(mN_h)\times p}, \tag{3.2}$$

ETNA
Kent State University and
Johann Radon Institute (RICAM)

and the matrix

$$\mathcal{V} = S - \frac{1}{p}\sum_{i=1}^{p}\left[\mathbf{u}_m(\alpha_i), \mathbf{u}_m(\alpha_i), \ldots, \mathbf{u}_m(\alpha_i)\right] \in \mathbb{R}^{(mN_h)\times p}$$

characterized by a null average. Matrix $\mathcal{V}$ is the array actually employed to extract the POD basis. For this purpose, we apply the Singular Value Decomposition (SVD) to $\mathcal{V}$, to obtain

$$\mathcal{V} = \Phi\Sigma\Psi^T, \tag{3.3}$$

where $\Phi \in \mathbb{R}^{(mN_h)\times(mN_h)}$ and $\Psi \in \mathbb{R}^{p\times p}$ are the unitary matrices gathering the left and the right singular vectors of $\mathcal{V}$, while $\Sigma = \text{ diag }(\sigma_1, \ldots, \sigma_\gamma) \in \mathbb{R}^{(mN_h)\times p}$ is the pseudo-diagonal matrix of the singular values of $\mathcal{V}$, with $\sigma_1 \geq \sigma_2 \geq \cdots \geq \sigma_\gamma \geq 0$ and $\gamma = \min(mN_h, p)$ [13]. In the numerical assessment below, we always assume $\gamma = p$.

The decomposition (3.3) allows us to define the POD orthogonal reduced basis, being the set of the first l most significant left singular vectors, $\{\boldsymbol{\phi}_i\}_{i=1}^{l}$, of $\mathcal{V}$, so that the reduced POD space is $V_{\text{POD}}^l = \text{span}\{\boldsymbol{\phi}_1, \ldots, \boldsymbol{\phi}_l\}$, with $\dim(V_{\text{POD}}^l) = l$ and, in general, $l \ll mN_h$.
As to the choice of the integer l, different criteria can be adopted. For instance, one can analyze the trend of the spectrum Σ or introduce a control on the variance, by selecting the first l ordered singular values such that

$$R_l = \frac{\sum_{i=1}^{l}\sigma_i^2}{\sum_{i=1}^{p}\sigma_i^2} \geq \epsilon, \tag{3.4}$$

for a positive user-defined tolerance ϵ [36].

REMARK 3.1. As an alternative to the procedure above, the POD basis can be derived by applying the spectral decomposition to the covariance matrix $C = \mathcal{V}^T\mathcal{V} \in \mathbb{R}^{p\times p}$, being assumed $p \ll mN_h$. In particular, it holds that $\lambda_i = \sigma_i^2$, and $\boldsymbol{\phi}_i = \lambda_i^{-1}S\mathbf{c}_i$, where $\{\lambda_i, \mathbf{c}_i\}$ denotes the generic {eigenvalue, eigenvector} pair associated with C, for $i = 1, \ldots, p$ [36].

REMARK 3.2 (Snaphot choice). The choice of representative values for the parameter α in (3.2) is a critical issue to make POD effective in practice. In general, it strictly depends on the problem at hand. In particular, the model reduction is effective if the selected snapshots cover the whole parameter space. This aspect is beyond the goal of this work, albeit extremely interesting.

Now, the *online phase* approximates the HiMod solution to problem (2.1) for the value α^* of the parameter, with $\alpha^* \neq \alpha_i$ for $i = 1, \ldots, p$, at a lower computational cost with respect to directly solving the HiMod system (2.4) for $\alpha = \alpha^*$. For this purpose, we project system (2.4) onto the POD space, V_{POD}^l, by computing the POD stiffness matrix and right-hand side,

$$A_{\text{POD}}(\alpha^*) = (\Phi_{\text{POD}}^l)^T A_m(\alpha^*)\,\Phi_{\text{POD}}^l \in \mathbb{R}^{l\times l}, \quad \mathbf{f}_{\text{POD}}(\alpha^*) = (\Phi_{\text{POD}}^l)^T\mathbf{f}_m(\alpha^*) \in \mathbb{R}^l, \tag{3.5}$$

respectively, where matrix $\Phi_{\text{POD}}^l = [\boldsymbol{\phi}_1, \ldots, \boldsymbol{\phi}_l] \in \mathbb{R}^{(mN_h)\times l}$ collects the POD basis vectors by column, while $A_m(\alpha^*)$ and $\mathbf{f}_m(\alpha^*)$ are the HiMod stiffness matrix and right-hand side in (2.4). Then, we solve the POD system of order l

$$A_{\text{POD}}(\alpha^*)\mathbf{u}_{\text{POD}}(\alpha^*) = \mathbf{f}_{\text{POD}}(\alpha^*), \tag{3.6}$$

with $\mathbf{u}_{\text{POD}}(\alpha^*) = [u_{\text{POD},1}^{\alpha^*}, \ldots, u_{\text{POD},l}^{\alpha^*}]^T \in \mathbb{R}^l$. This allows us to approximate the HiMod solution $\mathbf{u}_m(\alpha^*)$ in (2.4) by using the POD basis as

$$\mathbf{u}_m(\alpha^*) \approx \mathbf{u}_{\text{HiPOD}}^l(\alpha^*) = \sum_{s=1}^{l} u_{\text{POD},s}^{\alpha^*}\boldsymbol{\phi}_s \in \mathbb{R}^{mN_h},$$

ETNA
Kent State University and
Johann Radon Institute (RICAM)

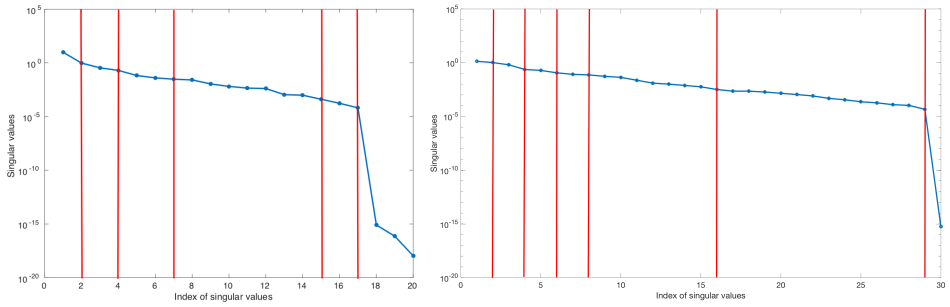

Fig. 3.1: Basic HiPOD reduction: singular values of matrix $\mathcal{V}$ for test case 3 (left) and 4 (right).

after solving a system of order l instead of mN_h. Finally, thanks to expansion (2.5), we obtain the HiPOD approximation $u^l_{\text{HiPOD}}(\alpha^*)$ to $u_m(x, \mathbf{y}; \alpha^*)$.
The assembly of $A_m(\alpha^*)$ and $\mathbf{f}_m(\boldsymbol{\alpha}^*)$ in (3.5) constitutes the bottleneck of the basic HiPOD method, although this represents a computational burden typical of any projection-based POD procedure. Nevertheless, the employment of a reduced rather than a full model when building matrix S leads to a considerable reduction of the computational effort, especially when m is a small value.

3.1.1. Numerical assessment. The basic HiPOD procedure is assessed on the test problems in Section 2.1.

Test case 3. To perform the offline phase, we assume an affine dependence of the problem data in (2.2) on the independent variables, x, y, so that

$$\mu(\mathbf{x}) = \mu_0 + \mu_x x + \mu_y y, \quad \mathbf{b}(\mathbf{x}) = [b_0 + b_x x, b_1 + b_y y]^T,$$
$$\sigma(\mathbf{x}) = \sigma_0 + \sigma_x x + \sigma_y y, \quad f(\mathbf{x}) = f_0 + f_x x + f_y y.$$

Then, we hierarchically reduce 30 different problems, by setting $\mu_0 = 1$, $\sigma_x = \sigma_y = 0$, $f_0 = 1$, and by randomly varying the remaining nine parameters as

$$\mu_x \in \mathcal{P}_{\mu_x} = [0,2], \quad \mu_y \in \mathcal{P}_{\mu_y} = [0,2], \quad \sigma_0 \in \mathcal{P}_{\sigma_0} = [0,3],$$
$$b_0 \in \mathcal{P}_{b_0} = [0,3], \quad b_1 \in \mathcal{P}_{b_1} = [0,3], \quad b_x \in \mathcal{P}_{b_x} = [0,2],$$
$$b_y \in \mathcal{P}_{b_y} = [0,2], \quad f_x \in \mathcal{P}_{f_x} = [-2,2], \quad f_y \in \mathcal{P}_{f_y} = [-2,2],$$

so that the parameter in (2.1) coincides with the vector $\boldsymbol{\alpha} = [\mu_x, \mu_y, \sigma_0, b_0, b_1, b_x, b_y, f_x, f_y]^T \in \mathbb{R}^9$ varying in $\mathcal{P} = \mathcal{P}_{\mu_x} \times \mathcal{P}_{\mu_y} \times \mathcal{P}_{\sigma_0} \times \mathcal{P}_{b_0} \times \mathcal{P}_{b_1} \times \mathcal{P}_{b_x} \times \mathcal{P}_{b_y} \times \mathcal{P}_{f_x} \times \mathcal{P}_{f_y}$.
The HiMod discretization uses linear FE along the mainstream, associated with a uniform partition of Ω_{1D} into 60 subintervals, and a modal expansion based on 10 sinusoidal modes. Figure 3.1, left shows the spectrum of matrix $\mathcal{V}$, where the vertical lines identify the dimension l for the POD space adopted in the online phase. The singular values decrease rather slowly until a drop occurs at $l = 17$ (being rank($\mathcal{V}$)=17). This can be ascribed to the large number of parameters involved, which limits the redundancy across the snapshots. During the online phase we approximate the same problem as in Section 2.1.1, for

$$\boldsymbol{\alpha}^* = [0,0,0,3,0,0,0,-2,3]^T \in \mathcal{P},$$

so that the reference HiMod solution is the one in Figure 2.1, bottom-right. Starting from the spectrum on the left side of Figure 3.1, we pick $l = 2, 4, 7, 15, 17$. The corresponding

ETNA
Kent State University and
Johann Radon Institute (RICAM)

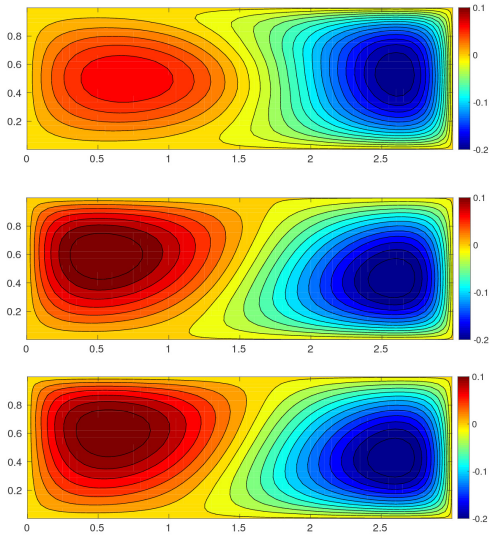

Fig. 3.2: Basic HiPOD reduction (test case 3): HiPOD approximation for $l = 2$ (top), $l = 7$ (middle) and $l = 15$ (bottom).

value for the ratio R_l in (3.4) is given by 0.9352, 0.9832, 0.9952, 0.9999, 1, respectively. Figure 3.2 provides the contour plots of $u^l_{\text{HiPOD}}(\boldsymbol{\alpha}^*)$ for $l = 2, 7, 15$. Solutions $u^2_{\text{HiPOD}}(\boldsymbol{\alpha}^*)$ and $u^7_{\text{HiPOD}}(\boldsymbol{\alpha}^*)$ exhibit a good accuracy if we take into account that they are obtained by solving a system of dimensionality 2 and 7, respectively and that we are varying 9 parameters, contemporarily. The quality of the HiPOD approximation gradually improves by increasing the dimension of the POD space, as confirmed also by the values in Table 3.1 which gathers the $L^2(\Omega)$- and of the $H^1(\Omega)-$norm of the relative modeling error obtained by replacing the HiMod solution $u_{10}(\boldsymbol{\alpha}^*)$ with the HiPOD approximation $u^l_{\text{HiPOD}}(\boldsymbol{\alpha}^*)$, for different values of l. The modeling error quickly reduces by increasing l. From a qualitative viewpoint, the HiPOD approximation $u^{15}_{\text{HiPOD}}(\boldsymbol{\alpha}^*)$ is fully comparable with the HiMod approximation in Figure 2.1, bottom-right with a reduction of the wall-clock time from 1.44 to 0.04 seconds* (the time associated with the HiPOD approximation refers to the online phase only).

	$l = 2$	$l = 4$	$l = 7$	$l = 15$	$l = 17$
$L^2(\Omega)$-norm	3.23e-01	5.98e-02	3.51e-02	2.70e-03	1.71e-03
$H^1(\Omega)$-norm	4.50e-01	1.23e-01	6.21e-02	7.61e-03	4.81e-03

Table 3.1: Basic HiPOD reduction (test case 3): relative modeling error for different HiPOD approximations.

Test case 4. As reference setting, we consider now the test case in Section 2.1.2. We adopt the following dependence on the independent variables for the problem data in (2.1),

$$\mu(\mathbf{x}) = \mu_0 + \mu_x x + \mu_y y, \quad \mathbf{b}(\mathbf{x}) = [b_0, b_1 \sin(6x)]^T,$$
$$\sigma(\mathbf{x}) = \sigma_0 + \sigma_x x + \sigma_y y, \quad f(\mathbf{x}) = f_1 \chi_{C_1}(\mathbf{x}) + f_2 \chi_{C_2}(\mathbf{x}).$$

*The computations have been run on a MacBookPro15,3 Intel Core i9 2.40GHz 32 GB desktop computer.

ETNA
Kent State University and
Johann Radon Institute (RICAM)

During the offline phase, we compute the HiMod approximation for 30 different ADR problems by setting $\mu_x = \mu_y = \sigma_x = \sigma_y = 0$, and by randomly varying

$$\mu_0 \in \mathcal{P}_{\mu_0} = [0.1, 10], \qquad b_0 \in \mathcal{P}_{b_0} = [2, 20], \qquad b_1 \in \mathcal{P}_{b_1} = [1, 3],$$
$$\sigma_0 \in \mathcal{P}_{\sigma_0} = [0, 3], \qquad f_1 \in \mathcal{P}_{f_1} = [5, 25], \qquad f_2 \in \mathcal{P}_{f_2} = [5, 25],$$

so that the parameter in (2.1) is provided by the vector $\boldsymbol{\alpha} = [\mu_0, b_0, b_1, \sigma_0, f_1, f_2]^T$ taking values in the set $\mathcal{P} = \mathcal{P}_{\mu_0} \times \mathcal{P}_{b_0} \times \mathcal{P}_{b_1} \times \mathcal{P}_{\sigma_0} \times \mathcal{P}_{f_1} \times \mathcal{P}_{f_2}$. The HiMod discretization employs linear FE on a uniform partition of Ω_{1D} into 120 subintervals, combined with 20 sinusoidal modes to discretize the transverse dynamics. Figure 3.1, right shows the trend of the spectrum for the corresponding matrix $\mathcal{V}$. This is characterized by a very slow decay, without any significant drop before the 29-th singular value (being $\mathrm{rank}(\mathcal{V}) = 29$).

The online phase is employed to approximate the solution to the problem in Section 2.1.2. This is equivalent to set the parameter to

$$\boldsymbol{\alpha}^* = [0.24, 5, 1, 0.1, 10, 10]^T \in \mathcal{P}.$$

Figure 3.3, top-bottom shows the basic HiPOD approximations $u^2_{\mathrm{HiPOD}}(\boldsymbol{\alpha}^*)$, $u^6_{\mathrm{HiPOD}}(\boldsymbol{\alpha}^*)$, $u^{16}_{\mathrm{HiPOD}}(\boldsymbol{\alpha}^*)$. As expected, the ratio R_l becomes closer to 1 when l increases, being $R_2 = 0.6163$, $R_6 = 0.9158$, and $R_{16} = 0.9971$. Six POD modes suffice to recognize already the general trend of the HiMod solution, whereas the HiPOD approximation $u^{16}_{\mathrm{HiPOD}}(\boldsymbol{\alpha}^*)$, which is obtained by solving a system of order 16, is fully comparable with the HiMod approximation $u_5(\boldsymbol{\alpha}^*)$ in Figure 2.2, bottom, solution to a system of dimension 600. This leads to a significative saving in terms of computational effort, the wall-clock time reducing from 14.53 seconds for the HiMod approximation to 0.20 seconds when resorting to the basic HiPOD approach.

Finally, Table 3.2 provides some quantitative information about the accuracy of the basic HiPOD approximation, by collecting the $L^2(\Omega)$- and the $H^1(\Omega)$-norm of the relative modeling error with respect to the HiMod approximation $u_{20}(\boldsymbol{\alpha}^*)$. The error reduction is slightly slower compared with the values in Table 3.1, the trend of the solution being in such a case less trivial.

	$l = 2$	$l = 4$	$l = 6$	$l = 8$	$l = 16$	$l = 29$
$L^2(\Omega)$-norm	2.41e-01	2.12e-01	9.83e-02	3.42e-02	3.94e-03	1.23e-03
$H^1(\Omega)$-norm	3.23e-01	1.87e-01	1.15e-01	4.93e-02	9.31e-03	2.33e-03

Table 3.2: Basic HiPOD reduction (test case 4): relative modeling error for different HiPOD approximations.

3.2. The directional HiPOD approach. The directional HiPOD method still combines HiMod reduction with POD by more deeply exploiting the separation of variables underlying a HiMod discretization. In particular, the SVD is employed to erase the redundancy along the main stream and the transverse direction, separately. Then, the online phase is carried out by interpolating instead of projecting. This relieves us from assembling the HiMod stiffness matrix and right-hand side associated with the online parameter, as expected by (3.5).

The *offline phase* starts by collecting the information to build the response matrix. To this aim, we compute the HiMod discretization to problem (2.1) for p different values, α_i, of the

ETNA
Kent State University and
Johann Radon Institute (RICAM)

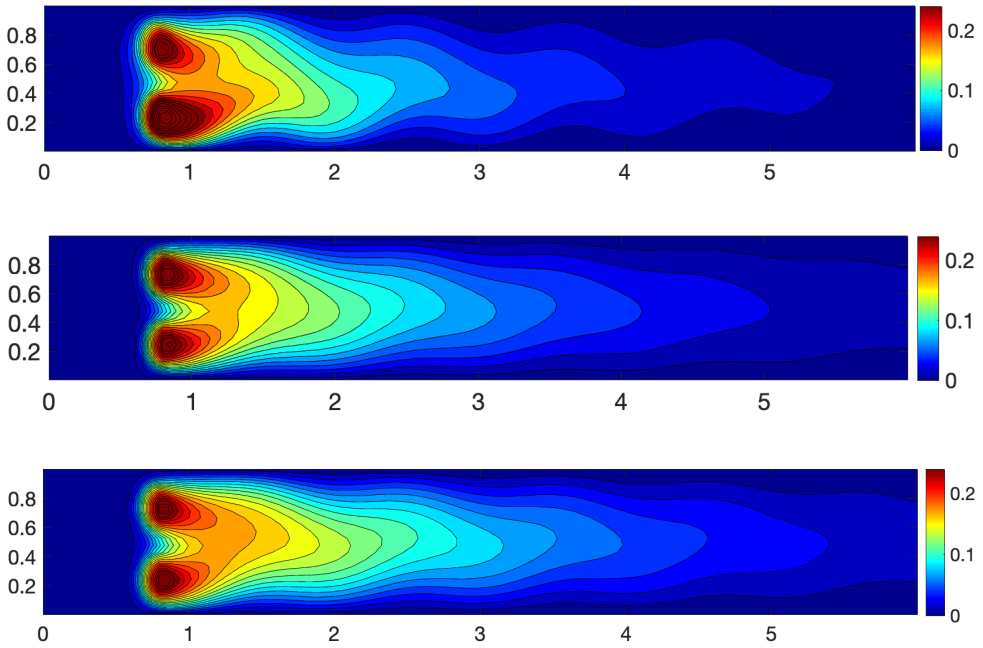

Fig. 3.3: Basic HiPOD reduction (test case 4): HiPOD approximation for $l = 2$ (top), $l = 6$ (center) and $l = 16$ (bottom).

parameter α, with $i = 1, \ldots, p$. The corresponding modal coefficients, $\{\widetilde{u}_{k,j}^{\alpha_i}\}_{k=1,j=1}^{m,N_h}$, are re-ordered by mode into the m vectors

$$\mathbf{U}^k(\alpha_i) = [\widetilde{u}_{k,1}^{\alpha_i}, \widetilde{u}_{k,2}^{\alpha_i}, \ldots, \widetilde{u}_{k,N_h}^{\alpha_i}]^T \in \mathbb{R}^{N_h} \quad k = 1, \ldots, m, \tag{3.7}$$

instead of in a unique vector as in (3.1). Then, we employ vectors $\mathbf{U}^k(\alpha_i)$ to assemble the response matrix

$$U = [\mathbf{U}^1(\alpha_1) \cdots \mathbf{U}^m(\alpha_1) \mid \mathbf{U}^1(\alpha_2) \cdots \mathbf{U}^m(\alpha_2) \mid \cdots\cdots\cdots \mid \mathbf{U}^1(\alpha_p) \cdots \mathbf{U}^m(\alpha_p)]$$

$$= \left[\begin{array}{ccc|ccc|c|ccc} \widetilde{u}_{1,1}^{\alpha_1} & \cdots & \widetilde{u}_{m,1}^{\alpha_1} & \widetilde{u}_{1,1}^{\alpha_2} & \cdots & \widetilde{u}_{m,1}^{\alpha_2} & \cdots & \widetilde{u}_{1,1}^{\alpha_p} & \cdots & \widetilde{u}_{m,1}^{\alpha_p} \\ \widetilde{u}_{1,2}^{\alpha_1} & \cdots & \widetilde{u}_{m,2}^{\alpha_1} & \widetilde{u}_{1,2}^{\alpha_2} & \cdots & \widetilde{u}_{m,2}^{\alpha_2} & \cdots & \widetilde{u}_{1,2}^{\alpha_p} & \cdots & \widetilde{u}_{m,2}^{\alpha_p} \\ \vdots & \vdots & \vdots & \vdots & \vdots & \vdots & \vdots & \vdots & \vdots & \vdots \\ \widetilde{u}_{1,N_h}^{\alpha_1} & \cdots & \widetilde{u}_{m,N_h}^{\alpha_1} & \widetilde{u}_{1,N_h}^{\alpha_2} & \cdots & \widetilde{u}_{m,N_h}^{\alpha_2} & \cdots & \widetilde{u}_{1,N_h}^{\alpha_p} & \cdots & \widetilde{u}_{m,N_h}^{\alpha_p} \end{array}\right].$$

Matrix $U \in \mathbb{R}^{N_h \times (mp)}$ exhibits a block-wise structure associated with the parameters α_i such that, for each block, columns run over modes while rows run over FE nodes. Now, we apply the SVD to matrix U, thus yielding

$$U = \Xi \Lambda K^T, \tag{3.8}$$

with $\Xi \in \mathbb{R}^{N_h \times N_h}$ and $K \in \mathbb{R}^{(mp)\times(mp)}$ unitary matrices, and $\Lambda \in \mathbb{R}^{N_h \times (mp)}$ a pseudo-diagonal matrix. The left singular vectors $\{\boldsymbol{\xi}_j\}_{j=1}^{N_h}$ of U constitute an orthogonal basis for

ETNA
Kent State University and
Johann Radon Institute (RICAM)

$\mathbb{R}^{N_h}$, so that each column of U can be expanded as

$$\mathbf{U}^k(\alpha_i) = \sum_{j=1}^{N_h} T_j^k(\alpha_i)\boldsymbol{\xi}_j \quad k = 1, \dots, m,\ i = 1, \dots, p. \tag{3.9}$$

In general, we can pick the first, say L with $L \leq N_h$, most meaningful singular vectors of U to identify the POD space, $V_{\text{POD},1}^L = \text{span}\{\boldsymbol{\xi}_1, \dots, \boldsymbol{\xi}_L\}$, associated with this first phase of the directional HiPOD procedure, being $\dim(V_{\text{POD},1}^L) = L$. Thus, vectors $\mathbf{U}^k(\alpha_i)$ can be approximated as

$$\mathbf{U}^k(\alpha_i) \cong \sum_{j=1}^{L} T_j^k(\alpha_i)\boldsymbol{\xi}_j \quad k = 1, \dots, m,\ i = 1, \dots, p, \tag{3.10}$$

where equality holds when $L = N_h$ (see (3.9)). Now, we re-organize coefficients $\{T_j^k(\alpha_i)\}$ by parameter, into the p vectors $\mathbf{T}_j(\alpha_i) = [T_j^1(\alpha_i), \dots, T_j^m(\alpha_i)]^T \in \mathbb{R}^m$ with $i = 1, \dots, p$, and we define the matrix

$$S_j = [\mathbf{T}_j(\alpha_1), \dots, \mathbf{T}_j(\alpha_p)] = \begin{bmatrix} T_j^1(\alpha_1) & \dots & T_j^1(\alpha_p) \\ \vdots & & \vdots \\ T_j^m(\alpha_1) & \dots & T_j^m(\alpha_p) \end{bmatrix} \in \mathbb{R}^{m \times p},$$

with $j = 1, \dots, L$. Then, we apply the SVD to each matrix S_j to obtain the L factorizations

$$S_j = R_j D_j P_j^T, \tag{3.11}$$

with $R_j \in \mathbb{R}^{m \times m}$ and $P_j \in \mathbb{R}^{p \times p}$ unitary matrices, and $D_j \in \mathbb{R}^{m \times p}$ the pseudo-diagonal matrix collecting the singular values of S_j. Thus, columns $\mathbf{T}_j(\alpha_i)$ of S_j can be represented in terms of the POD orthogonal basis $\{\mathbf{r}_j^k\}_{k=1}^{\mu_j}$, with $\mu_j \leq m$, constituted by the most significant μ_j left singular vectors of S_j, as

$$\mathbf{T}_j(\alpha_i) \cong \sum_{k=1}^{\mu_j} Q_j^k(\alpha_i)\mathbf{r}_j^k \quad j = 1, \dots, L,\ i = 1, \dots, p. \tag{3.12}$$

With each j, we associate the POD space $V_{\text{POD},2,j}^{\mu_j} = \text{span}\{\mathbf{r}_j^1, \dots, \mathbf{r}_j^{\mu_j}\}$, with $\dim(V_{\text{POD},2,j}^{\mu_j}) = \mu_j$. Thus, the directional HiPOD procedure yields $(L+1)$ POD bases which, during the online phase, are employed to predict the HiMod approximation to problem (2.1) for a new value, α^*, of the parameter, with $\alpha^* \neq \alpha_i$ for $i = 1, \dots, p$. For this purpose, first we compute an approximation for the coefficients $Q_j^k(\alpha^*)$ in (3.12), for $j = 1, \dots, L$ and $k = 1, \dots, \mu_j$, via a suitable interpolation of the (known) values $Q_j^k(\alpha_i)$ for $i = 1, \dots, p$; successively, we go through the directional procedure backward, until obtaining an approximation for the vector $\mathbf{U}^k(\alpha^*)$ in (3.7). In particular, thanks to (3.12), we compute the L vectors

$$\mathbf{T}_j(\alpha^*) = [T_j^1(\alpha^*), \dots, T_j^m(\alpha^*)]^T = \sum_{k=1}^{\mu_j} Q_j^k(\alpha^*)\mathbf{r}_j^k \quad j = 1, \dots, L \tag{3.13}$$

in $\mathbb{R}^m$, and then, according to (3.10), we assemble the m vectors $\mathbf{U}_{\text{HiPOD}}^k(\alpha^*) \in \mathbb{R}^{N_h}$ as

$$\mathbf{U}_{\text{HiPOD}}^k(\alpha^*) = [u_{\text{POD},k,1}^{\alpha^*}, \dots, u_{\text{POD},k,N_h}^{\alpha^*}]^T = \sum_{j=1}^{L} T_j^k(\alpha^*)\boldsymbol{\xi}_j \quad k = 1, \dots, m.$$

ETNA
Kent State University and
Johann Radon Institute (RICAM)

Finally, vectors $\mathbf{U}^k_{\text{HiPOD}}(\alpha^*)$ allow us to approximate the HiMod solution $u_m(\alpha^*)$ as

$$u_m(\alpha^*) \approx u^{L,M_L}_{\text{HiPOD}}(\alpha^*) = \sum_{k=1}^{m} \Big[\sum_{j=1}^{N_h} u^{\alpha^*}_{\text{POD},k,j} \vartheta_j(x) \Big] \varphi_k(\psi_x(\mathbf{y})),$$

with $M_L = \{\mu_j\}_{j=1}^{L}$, and where values $u^{\alpha^*}_{\text{POD},k,j}$ provide an approximation of the actual coefficient $\widetilde{u}^{\alpha^*}_{k,j}$ in (3.7) with $\alpha_i = \alpha^*$.

REMARK 3.3 (Choice of the interpolation). Different interpolation procedures can be adopted to compute coefficients $Q^k_j(\alpha^*)$. Following [37], we adopt a standard linear interpolation, a piecewise cubic Hermite interpolant and an interpolating radial basis function. In the next section, we numerically investigate the performances of these three approaches.

3.2.1. Numerical assessment. We numerically assess the reliability of the directional HiPOD procedure. First, we consider the case where α coincides with a single scalar quantity; then, we generalize the approach to the vector case, so that α will collect more parameters.

Test case 5. We adopt the solution to Test case 1 as the setting to be approximated during the online phase. The viscosity coefficient, μ, which is here assumed constant, represents the parameter driving the offline phase, so that $\alpha = \mu$. In particular, we hierarchically reduce problem (2.1)-(2.2) for 20 different values of μ, with $\mu = \mu_i$ uniformly sampled in the interval $\mathcal{P}_\mu = [0.15, 3]$ and $\mu_i \neq 1$ for $i = 1, \ldots, 20$, while preserving the same values as in (2.6) for the other problem data. The HiMod discretization is the same as adopted for Test case 3, so that we employ linear FE, associated with a uniform partition of Ω_{1D} into 60 subintervals, to discretize the main stream and 10 sinusoidal modes to describe the transverse dynamics.

Concerning the choice of L in (3.10) and of μ_i in (3.12), we resort to a control analogous to the one in (3.4). In more detail, for two fixed tolerances, ε_1 and ε_2, with $0 \leq \varepsilon_1, \varepsilon_2 \leq 1$, we preserve the first L left singular vectors, $\boldsymbol{\xi}_j$, of U and the first μ_j left singular vectors, $\mathbf{r}^k_j$, of S_j such that

$$R^L_{\text{POD},1} = \frac{\sum_{j=1}^{L} \lambda_j^2}{\sum_{j=1}^{N_h} \lambda_j^2} \geq \varepsilon_1 \quad \text{and} \quad R^{\mu_j}_{\text{POD},2} = \frac{\sum_{k=1}^{\mu_j} d_{j,k}^2}{\sum_{k=1}^{m} d_{j,k}^2} \geq \varepsilon_2, \tag{3.14}$$

respectively, with λ_j the singular value of U associated with $\boldsymbol{\xi}_j$ and $j = 1, \ldots, N_h$, and with $d_{j,k}$ the singular value of S_j corresponding to the k-th singular vector $\mathbf{r}^k_j$ and $k = 1, \ldots, m$. As a first check, we choose $\varepsilon_1 = \varepsilon_2 = \varepsilon$. In particular, Table 3.3 collects the predictions for L, for the maximum value and for the median of the values μ_j, for different choices of ε. As expected, the number of Hi-POD modes retained at both stages increases when ε approaches 1. Moreover, a slightly higher sensitivity of L to the selected tolerance is detected, when compared with the maximum value and the median of μ_j's.

	$\varepsilon = 0.6$	$\varepsilon = 0.9$	$\varepsilon = 0.99$	$\varepsilon = 0.999$	$\varepsilon = 0.9999$
L	1	3	5	7	10
$\max_j \mu_j$	4	6	8	9	10
median μ_j	2	4	6	8	8

Table 3.3: Directional HiPOD reduction (test case 5): prediction for the POD modes.

The online phase is performed by setting $\alpha^* = \mu^* = 1 \in \mathcal{P}_\mu$, and by using a radial basis function (RBF) interpolation [38]. In Figure 3.4, we compare the HiPOD approximations

ETNA
Kent State University and
Johann Radon Institute (RICAM)

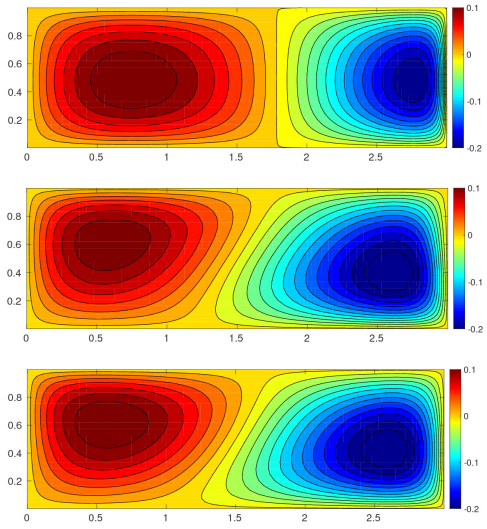

Fig. 3.4: Directional HiPOD reduction (test case 5): HiPOD approximation for $\varepsilon = 0.6$ (top), $\varepsilon = 0.9$ (middle) and $\varepsilon = 0.99$ (bottom).

associated with three of the selected tolerances. It is noticed that, at the first level of the procedure, at least three POD modes have to be adopted to have an approximation sufficiently reliable, which is equivalent to pick $\varepsilon \geq 0.9$. On average, the wall-clock time required by the directional HiPOD procedure is 0.08 seconds, which is significantly lower when compared with the time associated with the HiMod reduction in Section 2.1.1 (1.44 seconds for $m = 2$).

In Table 3.4, we analyze the convergence of the directional HiPOD approach, by computing the $L^2(\Omega)$- and the $H^1(\Omega)$-norm of the error yielded by replacing the HiMod solution $u_{10}(\alpha^*)$ with the HiPOD approximation. The accuracy ensured by the HiPOD approximation is remarkable if we consider that the values in the table refer to a relative error.

	$\varepsilon = 0.6$	$\varepsilon = 0.9$	$\varepsilon = 0.99$	$\varepsilon = 0.999$	$\varepsilon = 0.9999$
$L^2(\Omega)$-norm	4.66e-01	4.01e-02	3.11e-03	8.17e-04	1.37e-04
$H^1(\Omega)$-norm	4.62e-01	9.43e-02	1.05e-02	3.11e-03	5.71e-04

Table 3.4: Directional HiPOD reduction (test case 5): relative modeling error for different HiPOD approximations.

Finally, we run the directional HiPOD procedure by distinguishing the tolerances in (3.14), in order to identify a possible criterion of choice for ε_1 and ε_2. To this goal, we repeat the same error analysis as in Table 3.4, varying both ε_1 and ε_2 in the set of values $\{0.6, 0.9, 0.99, 0.999, 0.9999\}$. Table 3.5 collects the results of this invetigation. It turns out that the values of ε_1 and ε_2 have to be, in general, sufficiently close to 1 to have a monotonically decreasing trend of the error when we fix a tolerance and vary the other one. For this particular test case, a possible strategy to ensure this monotonicity can be to select ε_1 very close to 1 ($\varepsilon_1 = 0.9999$) and make ε_2 varying, or, as an alternative, we can fix ε_2 to 0.99, 0.999 or 0.9999 and gradually reduce the value for ε_1. This behaviour is shared by both the norms.

ETNA
Kent State University and
Johann Radon Institute (RICAM)

		$\varepsilon_2 = 0.6$	$\varepsilon_2 = 0.9$	$\varepsilon_2 = 0.99$	$\varepsilon_2 = 0.999$	$\varepsilon_2 = 0.9999$
$\varepsilon_1 = 0.6$	$L^2(\Omega)$-norm	2.58e-01	2.58e-01	2.57e-01	2.57e-01	2.57e-01
	$H^1(\Omega)$-norm	4.61e-01	4.61e-01	4.59e-01	4.59e-01	4.59e-01
$\varepsilon_1 = 0.9$	$L^2(\Omega)$-norm	5.43e-02	5.43e-02	2.01e-02	2.01e-02	2.01e-02
	$H^1(\Omega)$-norm	1.50e-01	1.50e-01	5.91e-02	5.88e-02	5.88e-02
$\varepsilon_1 = 0.99$	$L^2(\Omega)$-norm	3.73e-02	3.47e-02	5.80e-03	5.80e-03	5.80e-03
	$H^1(\Omega)$-norm	8.90e-02	7.57e-02	2.83e-02	2.83e-02	2.83e-02
$\varepsilon_1 = 0.999$	$L^2(\Omega)$-norm	3.72e-02	3.46e-02	1.34e-03	6.03e-04	6.03e-04
	$H^1(\Omega)$-norm	8.85e-02	7.51e-02	4.01e-03	3.10e-03	2.91e-03
$\varepsilon_1 = 0.9999$	$L^2(\Omega)$-norm	3.72e-02	3.46e-02	1.20e-03	5.57e-04	8.03e-05
	$H^1(\Omega)$-norm	8.84e-02	7.50e-02	2.81e-03	1.21e-03	3.95e-04

Table 3.5: Directional HiPOD reduction (test case 5): sensitivity to the selected tolerances.

Test case 6. The benchmark configuration is now provided by Test case 2, where the HiPOD parameter α, coincides with the reactive coefficient σ that we assume constant.

The offline phase involves the hierarchically reduction of problem (2.1)-(2.2) for 30 different values of the reaction, uniformly sampled in the range $\mathcal{P}_\sigma = [0.02, 0.4]$, while all the other problem data in (2.7) are preserved. The HiMod discretization adopted during this stage uses linear FE along Ω_{1D}, in correspondence with a uniform partition of the supporting fiber into 120 subintervals, and 20 sinusoidal modes in the transverse direction, analogously to what done in Test case 4.

We set $\alpha^* = \sigma^* = 0.1 \in \mathcal{P}_\sigma$ in the online phase to recover the setting of interest. The spectrum truncation in (3.14) is first driven by a unique tolerance, by selecting $\varepsilon_1 = \varepsilon_2 = \varepsilon$.

The first row in Table 3.6 provides the number, L, of POD modes selected at the first level of the HiPOD procedure, for five different choices of ε. The values in the table highlight the presence of a strong redundancy. Indeed, L is considerably lower with respect to N_h ($= 120$), even when ε is very close to 1. For instance, it suffices that the POD space $V^L_{\mathrm{POD},1}$ has a dimension equal to 12, to correctly describe the dynamics along the main stream. This is shown in Figure 3.5 which gathers the contour plots of the HiPOD approximation associated with the first four values selected for ε. Information about the values predicted for dimensions μ_j in (3.12) are also furnished by Table 3.6.

The configuration explored in this test case is more complex with respect to the one in Test case 5. This is confirmed by the larger number of POD modes ($L = 12$ versus $L = 3$) employed at the first level to ensure a reliable HiPOD solution. Despite that, also for this test case we have a computational gain with respect to the HiMod discretization in Section 2.1.2 (case $m = 5$). Indeed, the wall-clock time characterizing the directional HiPOD procedure is 0.33 seconds to be compared with 14.53 seconds for the HiMod reduction.

	$\varepsilon = 0.6$	$\varepsilon = 0.9$	$\varepsilon = 0.99$	$\varepsilon = 0.999$	$\varepsilon = 0.9999$
L	2	3	4	12	17
$\max_j \mu_j$	5	8	9	10	10
median μ_j	4	5	6	7	7

Table 3.6: Directional HiPOD reduction (test case 6): prediction for the POD modes.

ETNA
Kent State University and
Johann Radon Institute (RICAM)

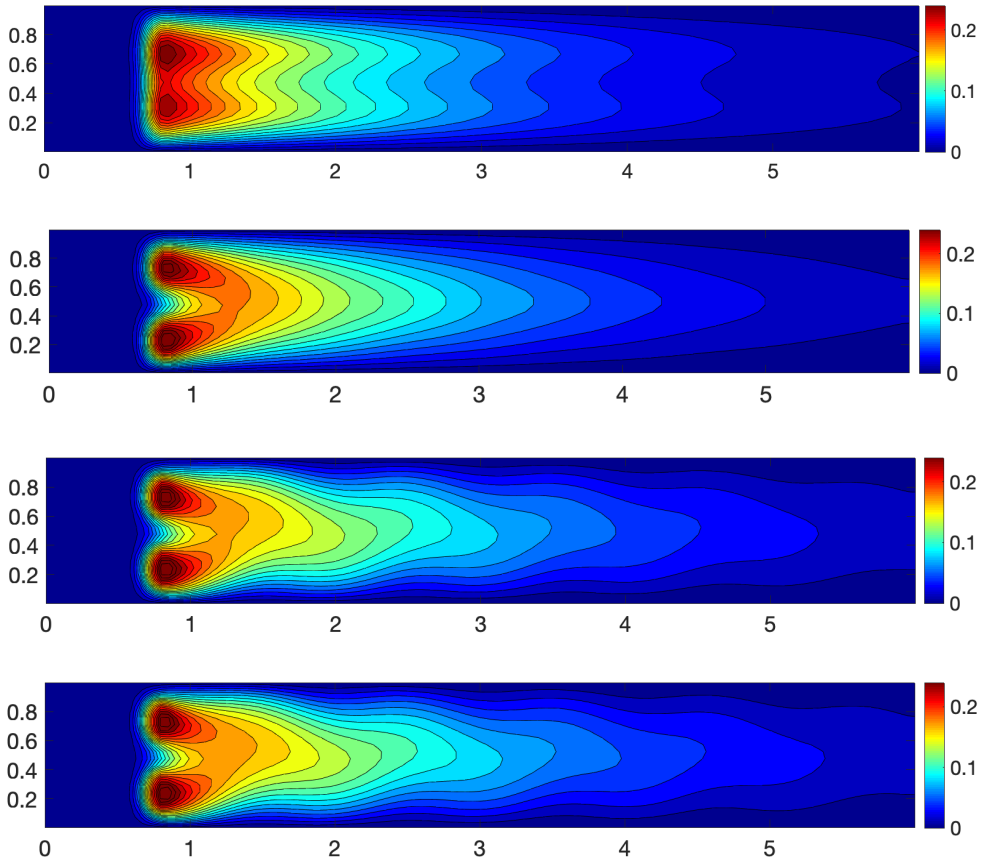

Fig. 3.5: Directional HiPOD reduction (test case 6): HiPOD approximation for $\varepsilon = 0.6, 0.9, 0.99, 0.999$ (top-bottom).

	$\varepsilon = 0.6$	$\varepsilon = 0.9$	$\varepsilon = 0.99$	$\varepsilon = 0.999$	$\varepsilon = 0.9999$
$L^2(\Omega)$-norm	1.93e-01	7.38e-02	1.16e-02	4.82e-04	5.54e-05
$H^1(\Omega)$-norm	4.34e-01	1.52e-01	3.08e-02	3.11e-03	3.84e-04

Table 3.7: Directional HiPOD reduction (test case 6): relative modeling error for different HiPOD approximations.

The accuracy of the directional HiPOD approximation is quantified in Table 3.7, in terms of the $L^2(\Omega)$- and of the $H^1(\Omega)$-norm of the POD relative error with respect to the HiMod solution $u_{20}(\alpha^*)$. The values in the table confirm the effectiveness of the directional HiPOD procedure.

Also for this test configuration, we explore the accuracy of the directional HiPOD approximation when we select different values for ε_1 and ε_2. The analysis in Table 3.7 is replicated, by assigning the values 0.6, 0.9, 0.99, 0.999, 0.9999 to both the tolerances. Table 3.8 provides the relative modeling error with respect to the reference HiMod solution in terms of the $L^2(\Omega)$- and of the $H^1(\Omega)$-norms. Conclusions similar to the ones for Table 3.5 can be drawn also for this test case. To ensure a monotonic trend for the error norm, it is fundamental to choose ε_1

ETNA
Kent State University and
Johann Radon Institute (RICAM)

very close to 1 ($\varepsilon_1 = 0.999$ or $\varepsilon_1 = 0.9999$) and gradually reduce ε_2, or, as an alternative, to set ε_2 to 0.99, 0.999 or 0.999, while diminishing ε_1.

		$\varepsilon_2 = 0.6$	$\varepsilon_2 = 0.9$	$\varepsilon_2 = 0.99$	$\varepsilon_2 = 0.999$	$\varepsilon_2 = 0.9999$
$\varepsilon_1 = 0.6$	$L^2(\Omega)$-norm	2.85e-01	2.85e-01	2.85e-01	2.85e-01	2.85e-01
	$H^1(\Omega)$-norm	3.81e-01	3.81e-01	3.81e-01	3.81e-01	3.81e-01
$\varepsilon_1 = 0.9$	$L^2(\Omega)$-norm	3.27e-02	3.27e-02	3.06e-02	3.06e-02	3.06e-02
	$H^1(\Omega)$-norm	6.49e-02	6.49e-02	6.45e-02	6.45e-02	6.45e-02
$\varepsilon_1 = 0.99$	$L^2(\Omega)$-norm	1.32e-02	1.21e-02	3.81e-03	3.81e-03	3.81e-03
	$H^1(\Omega)$-norm	1.47e-02	1.44e-02	1.23e-02	1.23e-02	1.23e-02
$\varepsilon_1 = 0.999$	$L^2(\Omega)$-norm	9.77e-03	8.75e-03	6.06e-04	6.04e-04	1.96e-04
	$H^1(\Omega)$-norm	1.27e-02	1.15e-02	1.18e-03	1.16e-03	1.21e-03
$\varepsilon_1 = 0.9999$	$L^2(\Omega)$-norm	9.73e-03	8.61e-03	5.81e-04	5.78e-04	8.68e-05
	$H^1(\Omega)$-norm	1.77e-02	1.15e-02	1.38e-03	1.31e-03	6.60e-04

Table 3.8: Directional HiPOD reduction (test case 6): sensitivity to the selected tolerances.

Finally, we use this test case to investigate the sensitivity of the directional HiPOD reduction procedure to the interpolant used in (3.13) to compute the coefficients $Q_j^k(\alpha^*)$. For this purpose, we come back to the configuration analyzed in Table 3.7 (i.e., we pick $\varepsilon_1 = \varepsilon_2 = \varepsilon$) and we consider the four largest values for the tolerance, $\varepsilon = 0.6$ providing an excessively poor approximation. According to Remark 3.3, we resort to a standard linear interpolation (LIN), a piecewise cubic Hermite (PCH) interpolant and to an interpolating RBF. Table 3.9 provides the $L^2(\Omega)$- and the $H^1(\Omega)$-norm of the relative error associated with the directional HiPOD approximation with respect to the HiMod solution $u_{20}(\alpha^*)$. For this test case, the PCH and the RBF interpolants slightly outperform the linear interpolation.

		$\varepsilon = 0.9$	$\varepsilon = 0.99$	$\varepsilon = 0.999$	$\varepsilon = 0.9999$
LIN	$L^2(\Omega)$-norm	7.38e-02	1.16e-02	4.83e-04	6.36e-05
	$H^1(\Omega)$-norm	1.52e-01	3.08e-02	3.11e-03	3.85e-04
PCH	$L^2(\Omega)$-norm	7.38e-02	1.16e-02	4.83e-04	5.54e-05
	$H^1(\Omega)$-norm	1.52e-01	3.08e-02	3.11e-03	3.84e-04
RBF	$L^2(\Omega)$-norm	7.38e-02	1.16e-02	4.82e-04	5.54e-05
	$H^1(\Omega)$-norm	1.52e-01	3.08e-02	3.11e-03	3.84e-04

Table 3.9: Directional HiPOD reduction (test case 6): sensitivity to the interpolant operator.

Test case 7. We analyze here the robustness of the directional HiPOD procedure in terms of extrapolation, to predict a scenario associated with a value, α^*, of the parameter out of the corresponding range $\mathcal{P}$. For this check, we select as reference configuration the solution to the ADR problem in (2.1)-(2.2) for the set of data

$$\begin{aligned} \mu(x,y) = 0.24, \quad \mathbf{b}(x,y) = [5, \sin(6x)]^T, \quad \sigma(x,y) = 0, \\ f(x,y) = 10\chi_{C1}(x,y) + 10\chi_{C2}(x,y), \end{aligned} \tag{3.15}$$

with C_1 and C_2 defined as in (2.7). From a qualitative viewpoint, the linear FE approximation to this problem is essentially identical to the solution in Figure 2.2, top, the reaction σ provid-

ETNA
Kent State University and
Johann Radon Institute (RICAM)

ing a negligible contribution to the solution trend.
Parameter α now coincides with the diffusivity coefficient μ. The offline phase involves the hierarchically reduction of problem (2.1)-(2.2) for ten different values of the viscosity, uniformly sampled in the range $\mathcal{P}_\mu = [1/30, 1]$, all the other problem data being preserved. The HiMod discretization adopted during this stage uses linear FE along Ω_{1D}, in correspondence with a uniform partition of the supporting fiber into 120 subintervals, and 20 sinusoidal modes along the transverse direction.
We pick $\alpha^* = 1/60 \notin \mathcal{P}_\mu$ as parameter characterizing the online stage. For comparison purposes, we adopt both the PCH and the RBF interpolations to compute coefficients $Q_j^k(\alpha^*)$ in (3.13). This choice is motivated by the higher reliability exhibited, in general, by these two interpolants in terms of extrapolation properties. Table 3.10 compares the modeling relative error associated with the two interpolants, in terms of the $L^2(\Omega)$- and the $H^1(\Omega)$-norms. PCH and RBF procedures are fully comparable, with a slightly better performance for the second interpolant. Figure 3.6 shows the contour plots of the reference HiMod solution, $u_{20}(\alpha^*)$, and of the directional HiPOD reduction when resorting to the RBF interpolant and for $\varepsilon_1 = \varepsilon_2 = \varepsilon = 0.9$ and 0.99 (tolerances $\varepsilon = 0.999, 0.9999$ provide contour plots very similar to the bottom panel). The challenge intrinsic into an extrapolation justifies the large values adopted for the tolerance. The matching between HiMod and HiPOD approximations is fulfilling.

		$\varepsilon = 0.9$	$\varepsilon = 0.99$	$\varepsilon = 0.999$	$\varepsilon = 0.9999$
PCH	$L^2(\Omega)$-norm	2.75e-01	1.01e-01	9.79e-02	9.78e-02
	$H^1(\Omega)$-norm	5.46e-01	2.13e-01	1.92e-01	1.92e-01
RBF	$L^2(\Omega)$-norm	2.67e-01	5.31e-02	4.70e-02	4.68e-02
	$H^1(\Omega)$-norm	5.36e-01	1.44e-01	1.02e-01	9.97e-02

Table 3.10: Directional HiPOD reduction (test case 7): robustness to extrapolation.

Test case 8. In this section we extend the HiPOD directional approach to the case when a multiple parameter has to be varied during the offline phase. The use of a vector of parameters leads us to modify the interpolation step of the procedure in Section 3.2. In particular, in order to recover coefficients $Q_j^k(\boldsymbol{\alpha}^*)$ in (3.13), we resort now to a two-dimensional interpolant.

As a reference differential setting, we adopt the ADR problem in Test case 7, where we identify the parameter with the vector $\boldsymbol{\alpha} = [\mu, b_1]^T$ which collects the diffusivity coefficient and the x-component of the advective field, $\mathbf{b} = [b_1, b_2]^T$, the y-component being preserved as in (3.15) (i.e., $b_2 = \sin(6x)$). The set of the admissible parameters is $\mathcal{P} = \mathcal{P}_\mu \times \mathcal{P}_{b_1}$, with $\mathcal{P}_\mu = [1/30, 1]$ and $\mathcal{P}_{b_1} = [0.5, 10]$.

Due to the higher dimensionality of the parameter space, we extend the sampling during the offline phase, by hierarchically reducing the reference ADR problem for $p = 600$ different choices of the parameter $\boldsymbol{\alpha}$. In particular, the interval $\mathcal{P}_\mu$ is sampled with 30 uniformly distributed points, whereas we pick 20 uniformly spaced points along the interval $\mathcal{P}_{b_1}$. The HiMod approximation coincides with the one adopted for Test case 7, which employs a linear finite element discretization associated with a uniform subdivision of Ω_{1D} into 120 subintervals along the mainstream, enriched by 20 sinusoidal modal functions to approximate the transverse dynamics.

The POD truncation is carried out by identifying the two tolerances in (3.14), and by setting $\varepsilon = \varepsilon_1 = \varepsilon_2 = 0.6, 0.9, 0.99, 0.999, 0.9999$.

ETNA
Kent State University and
Johann Radon Institute (RICAM)

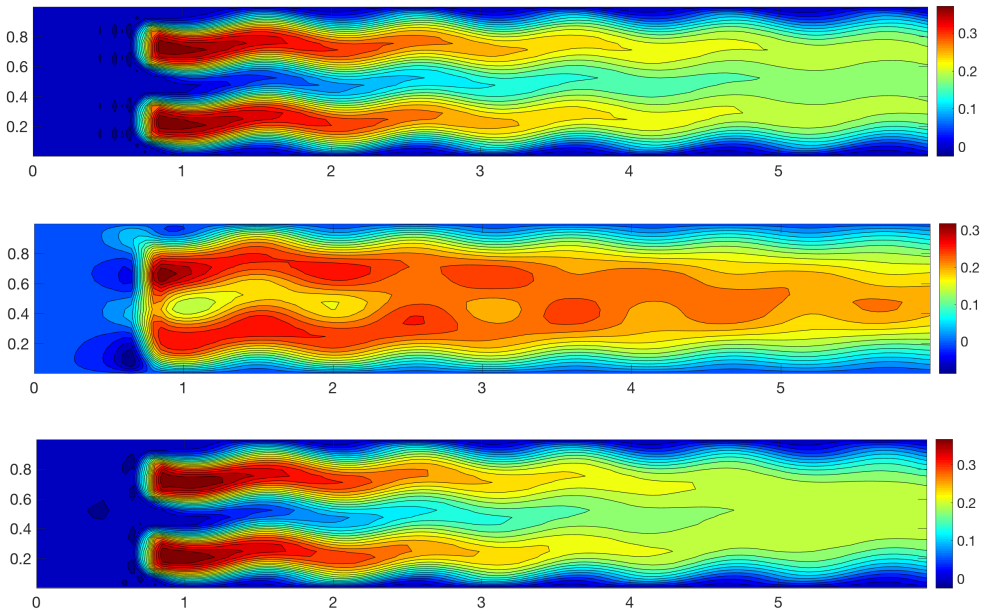

Fig. 3.6: Directional HiPOD reduction (test case 7): robustness to extrapolation. HiMod reference solution (top) and HiPOD approximation for $\varepsilon = 0.9$ (center) and $\varepsilon = 0.99$ (bottom).

The online phase is run to approximate the HiMod solution corresponding to the choices $\boldsymbol{\alpha}_1^* = [0.6, 5.1]^T$ and $\boldsymbol{\alpha}_2^* = [0.06, 9.3]^T$ for the parameter. Concerning the interpolation step, we adopt both the linear (LIN) and the piecewise cubic Hermite (PCH) bidimensional interpolant operators. In Figures 3.7 and 3.8 we compare the reference HiMod solutions, $u_{20}(\boldsymbol{\alpha}_1^*)$ and $u_{20}(\boldsymbol{\alpha}_2^*)$, with the approximation provided by the directional HiPOD reduction when combined with the PCH interpolation, and for the different tolerances. A tolerance sufficiently close to 1 has to be selected to obtain a reliable HiPOD solution. In particular, the choice α_2^* for the parameter turns out to be more challenging for the HiPOD procedure. This is confirmed also by a cross-comparison between the values in Tables 3.11 and 3.12, which gather the $L^2(\Omega)$- and the $H^1(\Omega)$-norm of the relative modeling error associated with the directional HiPOD approximation, together with other quantitative data. For the first choice of the parameter, $\boldsymbol{\alpha}_1^* = [0.6, 5.1]^T$, it is not immediate to appreciate a remarkable difference between the two interpolants, at least until the tolerance becomes very close to 1. Slightly better performances characterize the PCH interpolation for parameter $\boldsymbol{\alpha}_2^* = [0.06, 9.3]^T$, in particular with respect to the $L^2(\Omega)$-norm.

4. Basic versus directional HiPOD approach. This section has to be meant as an attempt of comparison between the two HiPOD procedures in Sections 3.1 and 3.2. This task turns out to be not so straightforward due to the strong heterogeneity between the two approaches. The actual goal is to identify specific configurations where one of the two HiPOD methods outperforms the other, rather than establishing which is the best formulation ever.

To make the comparison as fair as possible, we test the HiPOD reduction procedures by selecting the same parameters and corresponding range of variation. In particular:

i) we apply the basic HiPOD approach to the settings in Test cases 5 and 6;
ii) we replicate Test case 8 with the basic HiPOD approach for the choice α_1^*;

ETNA
Kent State University and
Johann Radon Institute (RICAM)

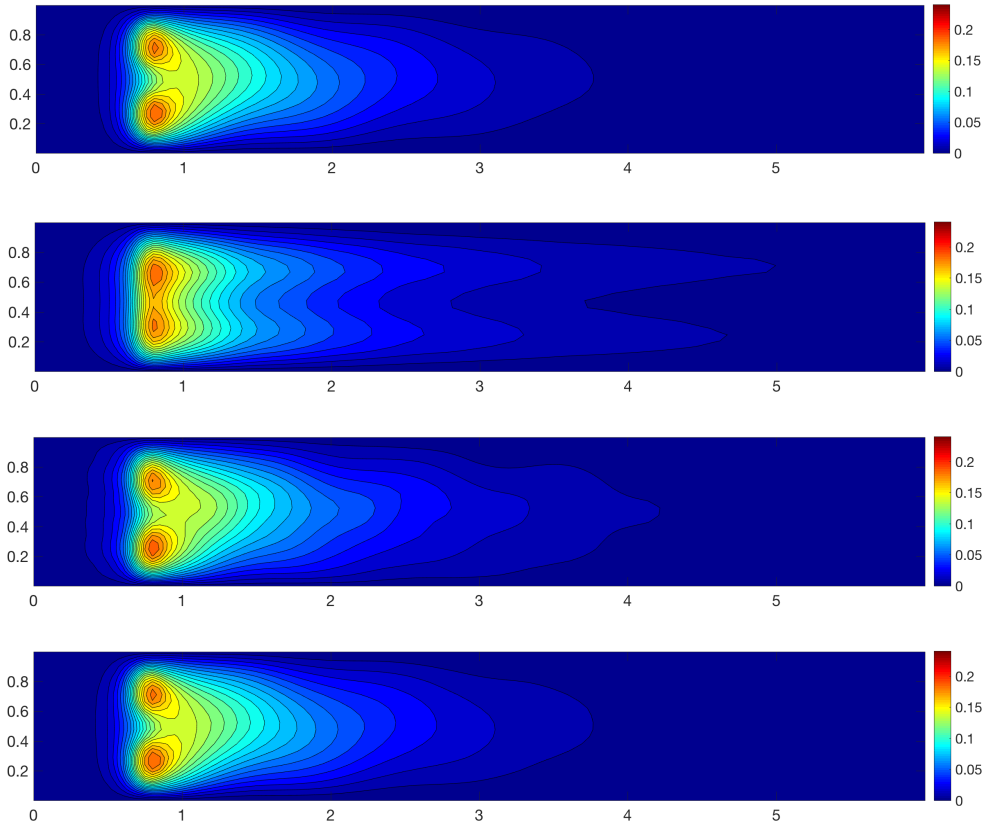

Fig. 3.7: Directional HiPOD reduction (test case 8) for $\boldsymbol{\alpha}_1^* = [0.6, 5.1]^T$: HiMod solution (first row) and HiPOD approximation associated with the PCH interpolant, and for $\varepsilon = 0.6$ (second row), $\varepsilon = 0.9$ (third row), $\varepsilon = 0.99$ (fourth row).

		$\varepsilon = 0.6$	$\varepsilon = 0.9$	$\varepsilon = 0.99$	$\varepsilon = 0.999$	$\varepsilon = 0.9999$
	L	2	6	16	32	41
	$\max_j \mu_j$	7	13	19	20	20
	median μ_j	5	10	16	19	20
LIN	$L^2(\Omega)$-norm	1.81e-01	5.13e-02	3.81e03	6.33e-04	5.71e-04
	$H^1(\Omega)$-norm	3.90e-01	1.37e-01	1.74e-02	2.10e-03	6.34e-04
PCH	$L^2(\Omega)$-norm	1.82e-01	5.13e-02	3.72e-03	2.78e-04	4.23e-05
	$H^1(\Omega)$-norm	3.90e-01	1.37e-01	1.74e-02	2.01e-03	2.51e-04

Table 3.11: Directional HiPOD reduction (test case 8): relative modeling error for different HiPOD approximations and sensitivity to the interpolant operator for $\boldsymbol{\alpha}_1^* = [0.6, 5.1]^T$.

iii) we customize a specific test case which highlights the potentialities of the directional method when the two levels of the procedure are properly exploited.

i). Test cases 5 and 6 are run with the basic HiPOD reduction procedure to approximate the HiMod solution in Section 2.1.1 and 2.1.2, respectively. In both cases, we deal with

ETNA
Kent State University and
Johann Radon Institute (RICAM)

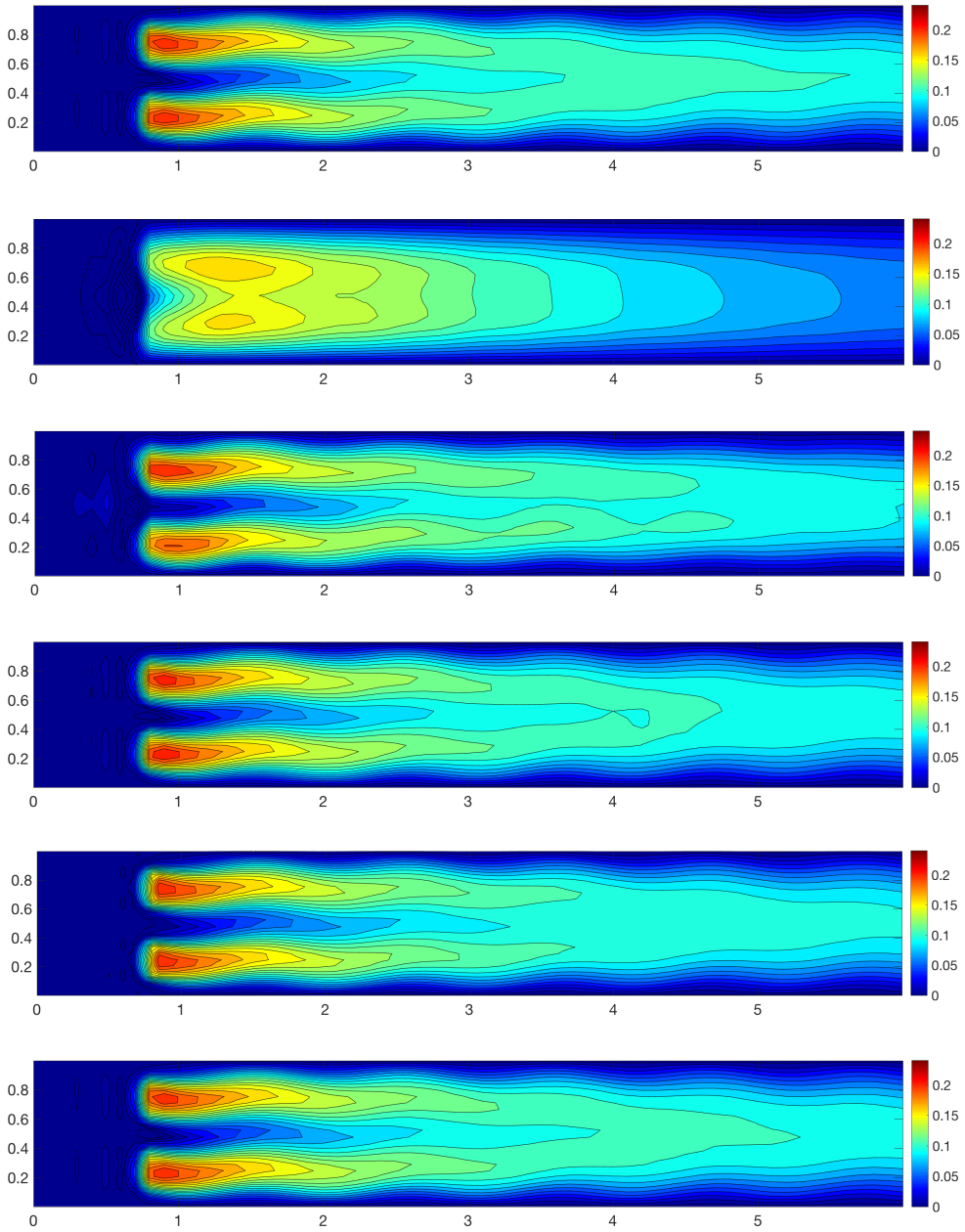

Fig. 3.8: Directional HiPOD reduction (test case 8) for $\boldsymbol{\alpha}_2^* = [0.06, 9.3]^T$: HiMod solution (first row) and HiPOD approximation associated with the PCH interpolant, and for $\varepsilon = 0.6$ (second row), $\varepsilon = 0.9$ (third row), $\varepsilon = 0.99$ (fourth row), $\varepsilon = 0.999$ (fifth row) and $\varepsilon = 0.9999$ (sixth row).

ETNA
Kent State University and
Johann Radon Institute (RICAM)

		$\varepsilon = 0.6$	$\varepsilon = 0.9$	$\varepsilon = 0.99$	$\varepsilon = 0.999$	$\varepsilon = 0.9999$
	L	2	6	16	32	41
	$\max_j \mu_j$	7	13	19	20	20
	median μ_j	5	10	16	19	20
LIN	$L^2(\Omega)$-norm	2.92e-01	5.89e-02	1.49e02	1.25e-02	1.25e-02
	$H^1(\Omega)$-norm	5.34e-01	1.73e-01	4.48e-02	2.76e-02	2.76e-02
PCH	$L^2(\Omega)$-norm	2.93e-01	5.76e-02	9.22e-03	4.30e-03	4.14e-03
	$H^1(\Omega)$-norm	5.24e-01	1.70e-01	3.62e-02	1.21e-02	9.53e-03

Table 3.12: Directional HiPOD reduction (test case 8): relative modeling error for different HiPOD approximations and sensitivity to the interpolant operator for $\boldsymbol{\alpha}_2^* = [0.06, 9.3]^T$.

	$l = 2$	$l = 4$	$l = 7$	$l = 10$	$l = 15$	$l = 17$
$L^2(\Omega)$-norm	1.91e-01	1.01e-02	9.29e-05	2.97e-07	9.24e-02	1.19e-01
$H^1(\Omega)$-norm	2.11e-01	1.14e-02	1.19e-04	5.22e-07	1.58e-01	1.89e-01

Table 4.1: Basic HiPOD reduction (test case 5): relative modeling error for different HiPOD approximations.

a single parameter setting which identifies α with the viscosity coefficient μ and with the reactive coefficient σ, respectively. We exploit the offline phase of the directional approach, by computing the HiMod solution for 20 and 30 values of the viscosity and of the reaction uniformly distributed in $\mathcal{P}_\mu = [0.15, 3]$ and in $\mathcal{P}_\sigma = [0.02, 0.4]$, respectively. The parameter α^* characterizing the online phase is $\alpha^* = \mu^* = 1$ for Test case 5 and $\alpha^* = \sigma^* = 0.1$ for Test case 6.

Tables 4.1 and 4.2 show the trend of the relative modeling error between the basic HiPOD approximation and the reference HiMod solutions, i.e., $u_{10}(\alpha^*)$ for Test case 5 and $u_{20}(\alpha^*)$ for Test case 6, when gradually increasing the dimension l of the POD basis.
Values in Table 4.1 highlight the performance of the basic HIPOD approach which allows us to gain some order of accuracy with respect to the directional procedure (see Tables 3.4 and 3.5), with a relative small number ($l = 10$) of POD modes. We observe also an unusual increment of both the errors for $l = 15$ and $l = 17$. This finds a justification in Figure 4.1 which shows the spectrum of matrix $\mathcal{V}$ in (3.3). Actually, the singular values in Σ drop to machine precision around the index 14-15, meaning that matrix $\mathcal{V}$ is numerically rank deficient. This implies that a POD reduction with truncated SVD with at most 15 components is enough to capture all the features of the parameter space. Additional components would disadvantage the reconstruction by injecting spurious terms due to numerical instabilities.
As far as Table 4.2 is concerned, we detect the expected decreasing monotonic trend of the error when measured in both the $L^2(\Omega)$- and the $H^1(\Omega)$-norm. A cross-comparison with Tables 3.7, 3.8 and 3.9 highlights that the directional HiPOD reduction outperforms for this case setting. Finally, the basic and the directional HiPOD procedures are essentially comparable in terms of computational effort, the wall-clock time being equal to 0.04 and 0.20 seconds for the basic approach to be compared with 0.08 and 0.33 seconds for the directional procedure, for Test case 5 and 6, respectively.

ii). We move to a multiparameter context, by considering Test case 8. We apply the basic HiPOD approach to approximate the HiMod solution associated with the parameter $\boldsymbol{\alpha}_1^* = [\mu^*, b_1^*]^T = [0.6, 5.1]^T$. We set up the offline phase as before for the directional

ETNA
Kent State University and
Johann Radon Institute (RICAM)

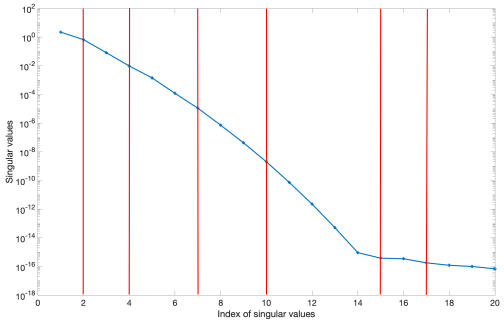

Fig. 4.1: Basic HiPOD reduction (test case 5): singular values of matrix $\mathcal{V}$.

	$l=2$	$l=4$	$l=6$	$l=8$	$l=10$
$L^2(\Omega)$-norm	7.33e-01	5.05e-01	7.36e-02	8.84e-03	7.54e-03
$H^1(\Omega)$-norm	8.33e-01	6.72e-01	8.09e-02	9.84e-03	9.34e-03

Table 4.2: Basic HiPOD reduction (test case 6): relative modeling error for different HiPOD approximations.

	$l=2$	$l=10$	$l=20$	$l=100$	$l=400$	$l=600$
$L^2(\Omega)$-norm	3.01e-01	2.22e-02	6.41e-03	5.80e-03	6.60e-04	2.43e-04
$H^1(\Omega)$-norm	4.56e-01	4.86e-02	8.12e-03	7.44e-03	9.48e-04	4.12e-04

Table 4.3: Basic HiPOD reduction (test case 8): relative modeling error for different HiPOD approximations for $\boldsymbol{\alpha}_1^* = [0.6, 5.1]^T$.

procedure, based on the HiMod solution to 600 different ADR problems, when uniformly varying parameter $\boldsymbol{\alpha} = [\mu, b_1]^T$ in the set of admissible parameters $\mathcal{P} = \mathcal{P}_\mu \times \mathcal{P}_{b_1} = [1/30, 1] \times [0.5, 10]$. To assess possible benefits of the basic approach in terms of accuracy, we compute the relative modeling error between the basic HiPOD approximation and the HiMod reference solution, $u_{20}(\alpha_1^*)$, for increasing values of l until all the POD modes are employed (namely, until $l = 600$). In Table 4.3, we collect the $L^2(\Omega)$- and the $H^1(\Omega)$-norm of such an error. A good accuracy is ensured also by the basic HiPOD procedure, provided that a sufficiently large number of POD modes is adopted. Nevertheless, the directional approach based on the PCH interpolant allows us to obtain an accuracy improvement by an order of magnitude with respect to the $L^2(\Omega)$-norm and without resorting to the full POD spectrum (see Table 3.11).

iii). Some comment on the role played by the two levels in the directional approach are in order to settle the new test case. The singular value decomposition of matrix U in (3.8) mixes information about the HiMod coefficients at different finite element nodes at the first level; on the other hand, the singular value decomposition of matrices S_j's in (3.11), at the second level, reveals a possible redundancy of information for the coefficients needed to describe the changes of the HiMod solution over different parameter configurations. Therefore, one would expect that mild changes of the HiMod coefficients across different values of the parameter lead to rank deficient matrices S_j's. This would translate into a potentially little

ETNA
Kent State University and
Johann Radon Institute (RICAM)

loss of accuracy when a dimensionality reduction is performed accordingly.

To support this conjecture, we set up a dedicated numerical test. At the i-th run of the offline phase, we solve in the domain $\Omega = (0, L_x) \times (0, L_y)$ a Poisson problem completed with homogeneous Dirichlet boundary conditions, so that the exact solution is

$$u_i(x, y) = x(x - L_x) \sum_{m=1}^{i} \sin\left(\frac{m\pi y}{L_y}\right).$$

The parameter governing the offline phase is the number i of HiMod modes used to reconstruct the solution u_i in exact arithmetic and, clearly, the complexity of the solution increases with i. Because solutions of different problems require a different number of HiMod modes, the accuracy of the HiPOD approximation is expected to be highly sensitive to the dimensionality reduction performed.
Now, we employ the online phase to recover the solution u_{i^*}, for a random value of the parameter i with $i = i^*$, via the directional HiPOD reduction, and we measure the associated (relative) error with respect to both the $L^2(\Omega)$- and the $H^1(\Omega)$-norm. Table 4.4 collects the results of such an analysis. The accuracy obtained with the HiPOD approximation is not sensitive to the threshold on the first level, but it is with respect to the threshold at the second level. This is reasonable, as the second level retains information about the importance of the HiMod modes in reconstructing the solution and how these modes vary through the parameter space spanned in the offline phase. Moreover, it can be noticed that matrices S_j's exhibit un upper triangular pattern, due to the growing complexity of the solution.

		$\varepsilon_2 = 0.6$	$\varepsilon_2 = 0.9$	$\varepsilon_2 = 0.99$
$\varepsilon_1 = 0.6$	$L^2(\Omega)$-norm	8.97e+00	2.54e+00	3.29e-04
	$H^1(\Omega)$-norm	9.16e+01	4.41e+01	4.99e-02
$\varepsilon_1 = 0.9$	$L^2(\Omega)$-norm	8.97e+00	2.54e+00	3.29e-04
	$H^1(\Omega)$-norm	9.16e+01	4.41e+01	4.99e-02
$\varepsilon_1 = 0.99$	$L^2(\Omega)$-norm	8.97e+00	2.54e+00	3.29e-04
	$H^1(\Omega)$-norm	9.16e+01	4.41e+01	4.99e-02

Table 4.4: Directional HiPOD reduction: relative modeling error for different choices of the tolerances to investigate the role of the two levels.

The basic HiPOD reduction is not conceived to work in such a combined way. Actually, by replicating the same test case, it can be checked that the error does not ever decrease below 5.52e-01 and 7.25e-01 with respect to the $L^2(\Omega)$- and the $H^1(\Omega)$-norm, respectively even when resorting to all the available POD modes.

5. Conclusions and developments. The numerical assessment in Sections 3.1.1 and 3.2.1 corroborates the reliability of the HiPOD reduction procedures. We have carried out a more extensive investigation on the directional approach, since it represents the main novelty of the paper. In particular, we have analyzed the performances of the directional HiPOD procedure in terms of convergence, selection of the tolerances driving the truncation of the POD bases, choice of the interpolant operator, and robustness with respect to extrapolation. Additionally, the numerical check carried out in the last section seems to suggest that the directional approach outperforms the basic one when dealing with phenomena characterized by a significative horizontal dynamics (i.e., in the considered test cases, by an advection field that dominates the diffusivity process).

ETNA
Kent State University and
Johann Radon Institute (RICAM)

Despite both the HiPOD procedures deserve a more thorough investigation in 3D and on more generic geometries, we believe that HiPOD model reduction represents a promising tool to effectively manage, for instance, multi-query contexts such as inverse problems, optimization strategies, data assimilation techniques, parameter estimation algorithms. This makes HiPOD a potential competitor against well-established techniques, such as the reduced basis method and the Proper Generalized Decomposition (PGD) (we refer to [27], where a first attempt of comparison between HiMod/HiPOD reduction and PGD is carried out).

Additionally, we highlight that the techniques here proposed are data-driven approaches so that they do not depend on the specific problem at hand. This could be of great usefulness with a view to complex applications. Moreover, HiPOD reduction procedures can be easily generalized by employing any reliable reduced model as the "truth", or by adopting methods other than POD to generate the reduced basis. In such a direction, in [39] the authors apply a reduced basis approach to collect the high-fidelity information and use a greedy algorithm to extract the essential information.

As for the possible future research topics, we mention the proposal of rigorous estimators to drive the POD selection ([18, 35]), the generalization of the HiPOD procedures to a nonlinear framework ([5, 17, 33]), the application of such techniques to concrete contexts, such as in hemodynamic modeling to help clinicians in taking operative decisions [8, 23].

Acknowledgements. This work used resources of the Oak Ridge Leadership Computing Facility (OLCF), which is a DOE Office of Science User Facility supported under Contract DE-AC05-00OR22725.

The second author acknowledges the European Union's Horizon 2020 research and innovation programme under the Marie Skłodowska-Curie Actions, grant agreement 872442 (ARIA, Accurate Roms for Industrial Applications), and the research project GNCS-INdAM 2020 "Tecniche Numeriche Avanzate per Applicazioni Industriali".

REFERENCES

[1] M.C. Aletti, S. Perotto, and A. Veneziani. HiMod reduction of advection-diffusion-reaction problems with general boundary conditions. *J. Sci. Comput.*, 76(1):89–119, 2018.

[2] D. Amsallem and C. Farhat. An online method for interpolating linear parametric reduced-order models. *SIAM J. Sci. Comput.*, 33(5):2169–2198, 2011.

[3] C. Audouze, F. De Vuyst, and P.B. Nair. Reduced-order modeling of parameterized PDEs using time-space-parameter principal. *Internat. J. Numer. Methods Engrg.*, 80(8):1025–1057, 2009.

[4] D. Baroli, C.M. Cova, S. Perotto, L. Sala, and A. Veneziani. Hi-POD solution of parametrized fluid dynamics problems: preliminary results. In *Model Reduction of Parametrized Systems*, volume 17 of *MS&A. Model. Simul. Appl.*, pages 235–254. Springer, Cham, 2017.

[5] M. Barrault, Y. Maday, N.C. Nguyen, and A.T. Patera. An empirical interpolation method: application to efficient reduced-basis discretization of partial differential equations. *C. R. Math. Acad. Sci. Paris*, 339(9):667–672, 2004.

[6] U. Baur, C.A. Beattie, P. Benner, and S. Gugercin. Interpolatory projection methods for parameterized model reduction. *SIAM J. Sci. Comput.*, 33(5):2489–2518, 2011.

[7] P. Benner, S. Gugercin, and K. Willcox. A survey of projection-based model reduction methods for parametric dynamical systems. *SIAM Rev.*, 57(4):483–531, 2015.

[8] Y.A. Brandes Costa Barbosa and S. Perotto. Hierarchically reduced models for the Stokes problem in patient-specific artery segments. *Int. J. Comput. Fluid Dyn.*, 34(2):160–171, 2020.

[9] C. Canuto, Y. Maday, and A. Quarteroni. Analysis of the combined finite element and Fourier interpolation. *Numer. Math.*, 39(2):205–220, 1982.

[10] F. Chinesta, R. Keunings, and A. Leygue. *The Proper Generalized Decomposition for Advanced Numerical Simulations: a Primer*. SpringerBriefs in Applied Sciences and Technology. Springer International Publishing, 2014.

[11] A. Ern and J.-L. Guermond. *Theory and Practice of Finite Elements*, volume 159 of *Applied Mathematical Sciences*. Springer-Verlag, New York, 2004.

ETNA
Kent State University and
Johann Radon Institute (RICAM)

[12] A. Ern, S. Perotto, and A. Veneziani. Hierarchical model reduction for advection-diffusion-reaction problems. In K. Kunisch, G. Of, and O. Steinbach, editors, *Numerical Mathematics and Advanced Applications*, pages 703–710. Springer-Verlag, Berlin Heidelberg, 2008.

[13] G.H. Golub and C.F. Van Loan. *Matrix Computations*. Johns Hopkins Studies in the Mathematical Sciences. Johns Hopkins University Press, Baltimore, MD, fourth edition, 2013.

[14] D. González and A. Ammar. Recent advances on the use of separated representations. *Internat. J. Numer. Methods Engrg.*, 81(5):637–659, 2010.

[15] S. Guzzetti, S. Perotto, and A. Veneziani. Hierarchical model reduction for incompressible fluids in pipes. *Internat. J. Numer. Methods Engrg.*, 114(5):469–500, 2018.

[16] Bernd Heinrich. The Fourier-finite-element method for Poisson's equation in axisymmetric domains with edges. *SIAM J. Numer. Anal.*, 33(5):1885–1911, 1996.

[17] J.S. Hesthaven, G. Rozza, and B. Stamm. *Certified Reduced Basis Methods for Parametrized Partial Differential Equations*. SpringerBriefs in Mathematics. Springer, Cham; BCAM Basque Center for Applied Mathematics, Bilbao, 2016.

[18] M. Hinze and M. Kunkel. Residual based sampling in POD model order reduction of drift-diffusion equations in parametrized electrical networks. *ZAMM Z. Angew. Math. Mech.*, 92(2):91–104, 2012.

[19] M. Kahlbacher and S. Volkwein. Galerkin proper orthogonal decomposition methods for parameter dependent elliptic systems. *Discuss. Math. Differ. Incl. Control Optim.*, 27(1):95–117, 2007.

[20] G. Kerschen, J. Golinval, A.F. Vakakis, and L.A. Bergman. The method of Proper Orthogonal Decomposition for dynamical characterization and order reduction of mechanical systems: an overview. *Nonlinear Dynam.*, 41(1-3):147–169, 2005.

[21] K. Kunisch and S. Volkwein. Galerkin proper orthogonal decomposition methods for parabolic problems. *Numer. Math.*, 148:117–148, 2001.

[22] K. Kunisch and S. Volkwein. Galerkin proper orthogonal decomposition methods for a general equation in fluid dynamics. *SIAM J. Numer. Anal.*, 40(2):492–515, 2002.

[23] L. Mansilla Alvarez, P. Blanco, C. Bulant, E. Dari, A. Veneziani, and R. Feijóo. Transversally enriched pipe element method (TEPEM): an effective numerical approach for blood flow modeling. *Int. J. Numer. Methods Biomed. Eng.*, 34(4):e02808, 2017.

[24] M. Ohlberger and K. Smetana. Approximation of skewed interfaces with tensor-based model reduction procedures: application to the reduced basis hierarchical model reduction approach. *J. Comput. Phys.*, 321:1185–1205, 2016.

[25] S. Perotto. Hierarchical model (Hi-Mod) reduction in non-rectilinear domains. In *Domain Decomposition Methods in Science and Engineering XXI*, volume 98 of *Lect. Notes Comput. Sci. Eng.*, pages 477–485. Springer, Cham, 2014.

[26] S. Perotto. A survey of hierarchical model (Hi-Mod) reduction methods for elliptic problems. In S.R. Idelsohn, editor, *Numerical Simulations of Coupled Problems in Engineering*, volume 33 of *Comput. Methods Appl. Sci.*, pages 217–241. Springer, Cham, 2014.

[27] S. Perotto, M.G. Carlino, and F. Ballarin. Model reduction by separation of variables: a comparison between Hierarchical Model reduction and Proper Generalized Decomposition. In S.J. Sherwin, D. Moxey, J. Peiró, P.E Vincent, and C. Schwab, editors, *Spectral and High Order Methods for Partial Differential Equations. ICOSAHOM 2018*, volume 134 of *Lect. Notes Comput. Sci. Eng.*, pages 61–77. Springer Nature Switzerland, 2020.

[28] S. Perotto, A. Ern, and A. Veneziani. Hierarchical local model reduction for elliptic problems: a domain decomposition approach. *Multiscale Model. Simul.*, 8(4):1102–1127, 2010.

[29] S. Perotto, A. Reali, P. Rusconi, and A. Veneziani. HIGAMod: a hierarchical isogeometric approach for model reduction in curved pipes. *Comput. & Fluids*, 142:21–29, 2017.

[30] S. Perotto and A. Veneziani. Coupled model and grid adaptivity in hierarchical reduction of elliptic problems. *J. Sci. Comput.*, 60(3):505–536, 2014.

[31] S. Perotto and A. Zilio. Hierarchical model reduction: three different approaches. In A. Cangiani, R.L. Davidchack, E. Georgoulis, A.N. Gorban, J. Levesley, and Tretyakov M.V., editors, *Numerical Mathematics and Advanced Applications*, pages 851–859. Springer-Verlag Berlin Heidelberg, 2013.

[32] S. Perotto and A. Zilio. Space-time adaptive hierarchical model reduction for parabolic equations. *Adv. Model. and Simul. in Eng. Sci.*, 2:25, 2015.

[33] A. Quarteroni, A. Manzoni, and F. Negri. *Reduced Basis Methods for Partial Differential Equations*, volume 92 of *Unitext*. Springer, Cham, 2016.

[34] M. Vogelius and I. Babuška. On a dimensional reduction method. I. The optimal selection of basis functions. *Math. Comp.*, 37(155):31–46, 1981.

[35] S. Volkwein. Optimality system POD and a-posteriori error analysis for linear-quadratic problems. *Control. Cybern.*, 291:1109–1125, 2011.

[36] S. Volkwein. Proper Orthogonal Decomposition: Theory and Reduced-Order Modelling. Lecture notes, University of Konstanz, 2013.

ETNA
Kent State University and
Johann Radon Institute (RICAM)

[37] S. Walton, O. Hassan, and K. Morgan. Reduced order modelling for unsteady fluid flow using proper orthogonal decomposition and radial basis functions. *Appl. Math. Model.*, 37(20-21):8930–8945, 2013.
[38] H. Wendland. Piecewise polynomial, positive definite and compactly supported radial functions of minimal degree. *Adv. Comput. Math.*, 4(4):389–396, 1995.
[39] M. Zancanaro, F. Ballarin, S. Perotto, and G. Rozza. Hierarchical model reduction techniques for flow modeling in a parametrized setting. *Multiscale Model. Simul.*, 19(1):267–293, 2021.